AN OFFSET ALLUVIAL FAN SOIL CHRONOSEQUENCE OF LITTLE ROCK CREEK ALONG THE MOJAVE SECTION OF THE SAN ANDREAS FAULT, LOS ANGELES COUNTY, CALIFORNIA

By

Carson Rittel

Submitted in partial fulfillment
of the requirements for the

Master of Science in Geology

Department of Earth and Environmental Science
New Mexico Institute of Mining and Technology

Socorro, New Mexico

September 2005

ABSTRACT

The use of soils has become increasingly important in estimating ages of deposits offset by strike-slip faulting. Soils chronosequence studies provide an alternative to more traditional methods and provide independent check on assumptions about surface stability and erosion rates used in other dating methods.

Soils formed on a set of five previously dated offset alluvial fans ranging in age from 29 – 413 ka near Little Rock Creek (LRC), CA show clay and iron oxide accumulation with increasing age. Soil morphologies on the fans also shows the development and thickening of argillic B-horizons. Iron oxide accumulation is less than in other regional studies due to decreased weathering, precipitation and temperature. Soils formed on topographic lows vary more than those from topographic highs. LRC soil development doesn't appear to be influenced by eolian sources. The chronosequence may also show the build up and eventual crossing of a pedogenic threshold on the oldest fan 5, based on a thinner than expected B-horizon thickness and less than expected clay and iron oxide accumulations. Fan 2 shows evidence of modification after deposition based on low clay and iron oxide accumulations.

Limitations in the chronosequence are due to few data points, soil variability across surfaces and uncertainties in calculated surface ages. However, the chronofunctions could be improved by the addition of more soil profiles, and in the future could be used to estimate ages of terraces cut into younger fan surfaces and strath terraces formed within the LRC watershed.

ACKNOWLEDGMENTS

I would like to thank my thesis committee; Drs. Bruce Harrison, Peter Mozley, and Dave Love for valuable suggestions during my time at New Mexico Tech. I would especially like to thank my advisor Bruce Harrison for initially suggesting this thesis work -- which has proved to be personally enjoyable. Bruce always has an open door and ear, which has made my graduate work much easier. I would also like to thank: Peter Fahnestock at the Natural Resources Conservation Service, Victorville, CA for donating valuable time and backhoe support for this study; New Mexico Tech's Graduate Student Association for partial funding through the 2004 and 2005 Matuszeski research grant and the 2005 travel grant; Bonnie Frey and Dustin Baca at the New Mexico Bureau of Geology for help with atomic absorption laboratory work; and Dr. Allan Barrows at the California Geologic Survey for providing digital map sources.

Special thanks to: Dr. Allan Ashworth (NDSU), Tiffany Borders, Dr. Mark Gonzalez (NDGS – US Forest Service), Elaine Hatzenbuhler (NDSU), Dr. Dave Johnson (NMT), Lisa Majkowski-Taylor, Dr. Bernie Saini-Eidukat (NDSU), Scooter Rittel (DOG), Dr. Donald Schwert (NDSU), KC Vorthmann, and Becca Walker.

TABLE OF CONTENTS

Page

ACKNOWLEDGMENTS ii

TABLE OF CONTENTS iii

LIST OF FIGURES v

LIST OF TABLES vii

LIST OF APPENDICES viii

PREFACE ix

INTRODUCTION 1

Regional soil chronosequences along the pedogenic gradient 3

Study Area and Previous Work 9

FIELD AND LABORATORY PROCEDURES 14

RESULTS 16

Soil Morphology and Clay content 16

Iron Oxide Analyses 17

DISCUSSION 31

Soil Morphology of Fan 5 35

Soils and erosion rates 37

Limitations of the chronosequence and estimated age of fan 2 38

Wider significance 41

CONCLUSIONS 44

REFERENCES 46

APPENDICES 50

LIST OF FIGURES

Page

Figure 1. Map of southern California showing locations of regional soil chronosequences along the pedogenic gradient. WC – Wilson Creek (Harden and Matti, 1989), STB – San Timoteo Badlands (Kendrick and McFadden, 1996), CP – Cajon Pass (McFadden and Weldon, 1987), LRC – Little Rock Creek (this study). Map datum is UTM, zone 11S, NAD27. 4

Figure 2. Location of study area in southern California along the San Andreas fault. The Little Rock Creek watershed is the largest drainage basin in the area at ~200 km^2. Circle symbols – location of soil profiles in this study (Appendix C; Table 7). A shutter ridge is found just NW of fan 0. Fan boundaries are modified from the geology of Barrows et al. (1985). Map datum is UTM, zone 11S, NAD27. 10

Figure 3. Soil development on topographic high surfaces. (A) Soil profile LRC 1 on fan 1 (29 ± 7 ka). (B) Soil profile LRC9 on fan 4 (281 ± 181 ka). Notice the differences between the soils of different ages. LRC 1 has a Bw-horizon, unweathered clasts while LRC9 has a thick well-developed argillic B-horizon, weathered clasts, and soil reddening due to iron oxide accumulation. Length of measuring tape is 1.4 m. 20

Figure 4. B-horizon thickness, maximum Fe_2O_3d percent, and profile mass Fe_2O_3d with increasing (log) age for dated fans at LRC. Solid lines are topographic high profiles and dashed lines are topographic low profiles..... 21

Figure 5. Topographic high soil profile LRC 11 from fan 5. Notice the lack of a fine-grained B-horizon. Length of measuring tape is 1.4 m..... 22

Figure 6. Example of a fine-grained topographic low soil (LRC 8) from fan 3. Length of measuring tape is 1.4 m. 23

Figure 7. Example of soil development with increasing age on topographic low soils, (A) Fan 2 topographic low soil LRC6 (no age). (B) Fan 5 topographic low soil LRC 12 (413 ± 185 ka). Notice the reddening of the profile with increasing age from the accumulation of iron oxides. Length of measuring tape is 1.4 m. 24

Figure 8. Changes in profile mass of clay for topographic highs and lows. (A) Profile mass of clay with increasing ages and resulting chronofunctions using dated fans 0, 1, 3, 4. Fan 5 was not used in the calculation of chronofunctions because of significant erosion. (B) Profile mass of clay with increasing depth for all fans. Notice the marked decrease of profile mass for fan 5. 25

Figure 9. Changes in profile mass of Fe_2O_3d for topographic highs and lows. (A) Profile mass of Fe_2O_3d with increasing ages and resulting chronofunctions using dated fans 0, 1, 3, 4. Fan 5 was not used in the calculation of chronofunctions because of increased erosion. (B) Profile mass of Fe_2O_3d with increasing depth for all fans. Notice the marked decrease of profile mass for fan 5. 26

Figure 10. Changes in profile mass of Fe_2O_3o for topographic highs and lows. (A) Profile mass of Fe_2O_3o with increasing ages and resulting chronofunctions using dated fans 0, 1, 3, 4. (B) Profile mass of Fe_2O_3o with increasing depth for all fans. Notice the marked decrease of profile mass for fan 5. 27

Figure 11. Relation between the ratio of profile clay verses Fe_2O_3d with time for topographic high surfaces. Fan 5 data were not used in the creation of the curve because of substantial erosion. 28

Figure 12. Relationship between profile mass of clay verses Fe_2O_3d for topographic high and low soil profiles. 30

LIST OF TABLES

Page

Table 1. Summary of soil-forming factors in the Cajon Pass, San Timoteo Badlands, Wilson Creek, and Little Rock Creek chronosequences.....5

Table 2. Summary of Soil Properties and Lab Results in the Little Rock Creek Soil Chronosequence 18

Table 3. Summary of fan parameters and estimated ages of fan 2 from solved soil chronofunctions and slip rate data.....40

Table 4. Fe_2O_3d and Fe_2O_3o Laboratory Data.....55

Table 5. Selected field and laboratory data used for and example calculation of horizon and profile mass.....59

Table 6. Expanded table of calculations for horizon and profile mass of sand, silt, clay, Fe_2O_3d, and Fe_2O_3o.....60

Table 7. Locations of soil profiles along offset alluvial fans near Little Rock, CA.....62

LIST OF APPENDICES

Page

APPENDIX A - Iron Oxide Extraction Methods and Laboratory Data.....49

APPENDIX B - Calculation of horizon and profile mass.....57

APPENDIX C - Fan Locations.....60

PREFACE

The results of this will be eventually published in an international journal (e.g., Quaternary *Research*, *Geomorphology*). I've written the text so that it adheres to the approximate 6000 word limit of these journals, with hopes of easy transition from thesis to journal format. The appendices include additional information on methods, data, and expanded tables not fully discussed in the main body of the text.

This thesis is accepted on behalf of the
Faculty of the Institute by the following committee:

J. G. Harrison

Advisor

David W. Love

Date

I release this document to the New Mexico Institute of Mining and Technology.

Student's Signature

9/9/2005

Date

INTRODUCTION

Soils have become increasingly important in correlation and relative age estimation of surficial deposits (McFadden and Weldon, 1987; Harden and Matti, 1989; Kendrick and McFadden, 1996). Soils are readily available and provide a means of age control when other datable material is limited, absent, or too costly to analyze. They also provide an independent check on numerically dated deposits. In strike-slip faulting environments, such as the San Andreas fault, offset geomorphic surfaces may be correlated by soil development (Harden and Matti, 1989). Accurate identification and correlation of offset surfaces are important in determining long term slip rates (Weldon and Sieh, 1985; Matmon et al., 2005). The degree of soil development also provides insight into landscape stability and erosion rate assumptions used in other dating methods (e.g., cosmogenic dating). For example, assumptions that overestimate boulder erosion rates in cosmogenic dating of offset deposits would lead to an overestimated age and an underestimated slip rate. On the other hand, an underestimated boulder erosion rate and age would result in an overestimated slip rate (Matmon et al., 2005).

Estimating ages of surficial deposits on the basis of soil development is accomplished through the development of a soil chronosequence. This assumes other major soil forming factors such as climate, vegetation, topography, and parent

material remain reasonably constant throughout soil formation (Jenny 1941, 1961). Undated and dated soils formed under similar soil forming factors are then correlated on the basis of soil development.

Soils formed on offset alluvial fans outside Little Rock Creek provide an opportunity to create a soil chronosequence along the Mojave segment of the San Andreas fault. Age control from cosmogenic dates and slip rates provide the framework for quantifying changes in soil development with time. However, age control is subject to uncertainties in age determination, offset distances, erosion rates, and slip rates. The purpose of this study was to construct a soil chronology of offset alluvial fans of Little Rock Creek where rates and processes of soil development including landscape stability, were evaluated with time. In addition, the soil chronosequence was used to estimate the age of an undated fan surface. In the future it will be used to provide age constraints on other surfaces in the area. Finally, the chronosequence provides additional information about the pedogenic gradient that extends in an east-west transect from the Mojave Desert to the Transverse Ranges of southern California (McFadden, 1982; Birkeland, 1985; McFadden and Weldon, 1987; Kendrick and McFadden, 1996). Pedogenic gradients are defined as variations in soil properties and processes along bioclimatic gradients and are identified from soil chronosequence studies (Tedrow, 1977; Birkeland, 1985).

Regional soil chronosequences along the pedogenic gradient

Several soil chronosequences are found along the southern California pedogenic gradient (Table 1; Fig. 1). These studies include the Cajon Pass (McFadden, 1982; McFadden and Hendricks, 1985; McFadden and Weldon, 1987; Harrison et al., 1990), Wilson Creek (Harden and Matti, 1989), and the San Timoteo Badlands (Kendrick and McFadden, 1996) chronosequences. Workers in this region have used soil development to estimate ages of surfaces using a combination of soil properties, morphology, development indices, and laboratory analyses. Even though studies have identified the southern California pedogenic gradient, several problems exist in quantifying changes that occur along this gradient. First, each chronosequence study usually has a different research objective. This leads to each study choosing different parameters to quantify soil development. For example, one study may use soil development indices (Harden and Matti, 1989), whereas another study may use soil chemistry (Kendrick and McFadden, 1996) to quantify soil development. This results in gaps in the understanding about changes in soil chemistry between the sites along the gradient. Another problem arises in using soil development indices between two different studies. Different workers can interpret soil properties differently, resulting in greater error in soil development indices. Although not addressed in this study, there needs to be a more standardized approach to future soil studies along the pedogenic gradient. This would result in a more

complete understanding of soil-forming processes along the southern California pedogenic gradient. Several southern California soil chronosequence studies are briefly summarized below.

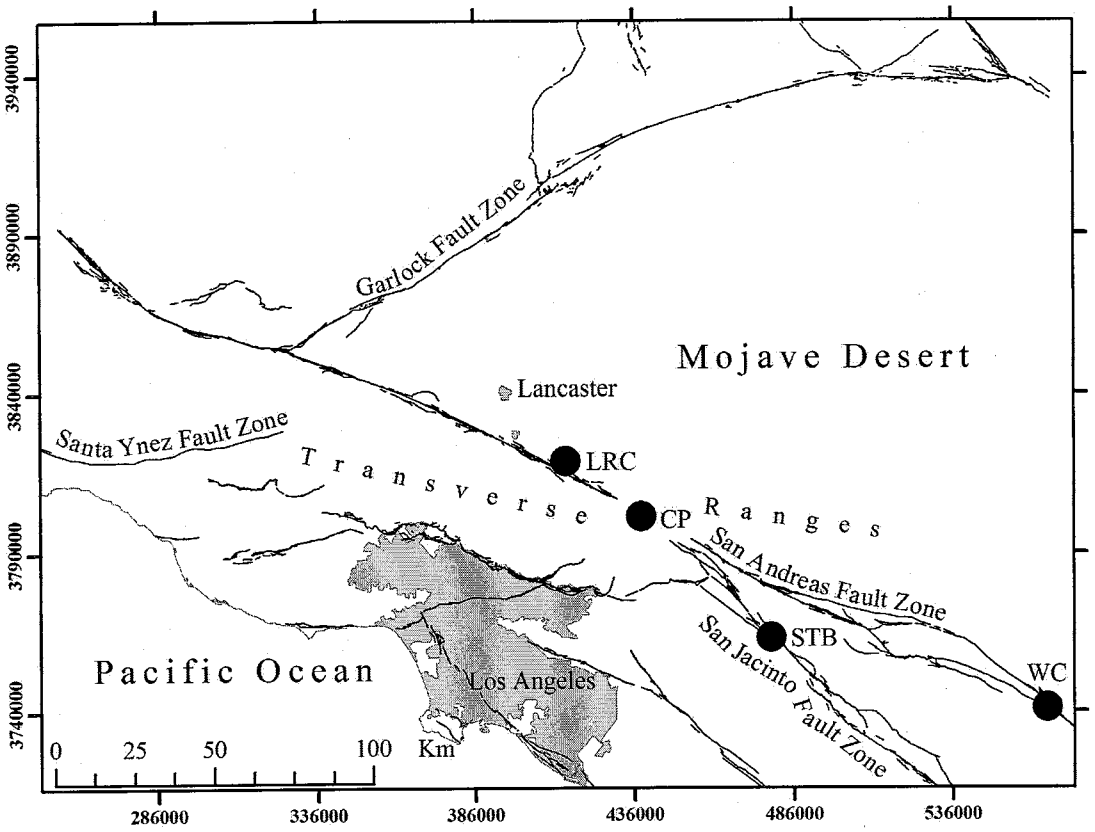

Figure 1. Map of southern California showing locations of regional soil chronosequences along the pedogenic gradient. WC – Wilson Creek (Harden and Matti, 1989), STB – San Timoteo Badlands (Kendrick and McFadden, 1996), CP – Cajon Pass (McFadden and Weldon, 1987), LRC – Little Rock Creek (this study). Map datum is UTM, zone 11S, NAD27.

Table 1. Summary of soil-forming factors in the Cajon Pass, San Timoteo Badlands, Wilson Creek, and Little Rock Creek chronosequences

Soil Study	Source	Climate	Parent Material	Mean Annual Temperature (°C)	Mean Annual Rainfall (cm)
Cajon Pass	McFadden and Weldon (1987)	Mediterranean	arkosic gravels/sands	16.5	60
San Timoteo Badlands	Kendrick and McFadden (1996)	Mediterranean	arkosic gravels/sands	17	36
Wilson Creek	Harden and Matti (1989)	Mediterranean	arkosic gravels/sands	15.8	75
Little Rock Creek	This study	Mediterranean	arkosic gravels/sands	12.1 - 17.2	16.8 - 27

Workers in the Cajon Pass chronosequence quantified soil development using soil morphology and profile masses of clay and pedogenic iron oxides (McFadden, 1982; McFadden and Hendricks, 1985; McFadden and Weldon, 1987). Surfaces at Cajon Pass range in age from 47 yr BP to 0.5 Ma and have been estimated from radiocarbon dates, paleomagnetism, and inferred constant slip rates. Results of the Cajon Pass chronosequence along with other studies showed that weight percent and profile mass of clay and iron oxides increase with time and can be used as an estimate of soil age (Bockeim, 1980; McFadden, 1982; Muhs, 1982; McFadden and Hendricks, 1985; Harden, 1987). The results of the chronosequence also identified eolian dust as the most important factor affecting Holocene soil development at Cajon Pass. As dust was incorporated into the soils at Cajon Pass, soils became less permeable which increased water holding capacity and accelerated rates of weathering.

Harden and Matti (1989) used soil development indices to estimate ages of offset alluvial fan deposits and to estimate slip along the San Andreas fault in the Wilson Creek chronosequence. To quantify soil development they used the profile development index of Harden (1982) and Harden and Taylor (1983) calibrated to the Cajon Pass (McFadden and Weldon, 1987) and the northern California Merced (Harden 1982) chronosequences. Soil development indices were created using texture, rubification, dry consistence, and clay films because these properties were found to best reflect soil age in the Central Valley of California (Harden and Taylor, 1983). Ages estimates of the surfaces were expected to have as much as 80% uncertainty based on poor calibration dates. Soils at Wilson Creek developed under similar soil-forming factors as Cajon Pass, but showed significantly less influence from eolian dust (Harden and Matti, 1989). The study also lacked soil chemistry data which would help to further constrain ages and further quantify the southern California pedogenic gradient.

Kendrick and McFadden (1996) compared soil processes in the San Timoteo Badlands with the Cajon Pass chronosequence using soil morphology, development indices and pedogenic iron oxides, contents of four terraces. When compared to the Cajon Pass chronosequence, the San Timoteo Badlands showed similar soil development but differences in pedogenic iron oxide content and decreased eolian dust influence. The San Timoteo Badlands also showed increased ferrihydrite

(oxalate extractable iron, Fe_2O_3o) content in depth profiles. Kendrick and McFadden (1996) attributed increased Fe_2O_3o content from lower precipitation in the San Timoteo Badlands. This would result in less soil leaching, weathering, and slower conversion of ferrihydrite (Fe_2O_3o) into more stable hematite (dithionite extractable iron, Fe_2O_3d). The lower precipitation rate also was suggested as the cause of accumulation of silica in the soils. Silica accumulation would inhibit the transformation of Fe_2O_3o into Fe_2O_3d. The study also showed differences in the amounts of eolian influence between the sites. Decreased eolian input would result in a decreased water holding capacity of the soils when compared to Cajon Pass soils. This would lead to lower soil leaching, weathering, and secondary clay development at the San Timoteo Badlands.

When evaluating the previous body of work of southern California soil studies, the most useful indicators of soil development with time are soil morphology and the accumulation of weathering products such as iron oxides and clay within a given soil profile. As soils increase in age, profiles should also increase in B-horizon thickness and accumulated products of chemical weathering. These parameters of soil development are easily quantified using field observations and laboratory analyses. Soil development indices are also important tools, but are not always available for each study.

Pedogenic iron oxyhydroxides (referred to hereafter as oxides for brevity) have been used as indicators of soil age (McFadden, 1982; McFadden and Hendricks, 1985; Birkeland, 1989).These pedogenic iron oxides are formed from the oxidation of unstable mafic minerals within soil parent material and increase as a function of soil age. Initially precipitated pedogenic iron oxides form poorly crystalline or amorphous ferrihydrite (Fe_2O_3o) and with time transform to more crystalline and thermodynamically stable hematite or goethite (McFadden, 1982; McFadden and Hendricks, 1985; Schwertmann, 1993). This conversion of ferrihydrite to hematite accounts for the reddening or rubification of a soil with age. The type of pedogenic iron oxides also changes with increasing soil age. McFadden (1982) demonstrated the amount of Fe_2O_3o within a soil chronosequence eventually reaches a maximum value and then decreases with increasingly older soils. The eventual decrease in Fe_2O_3o is due to the continued conversion of ferrihydrite to more stable hematite.

The accumulation of authigenic clay has also used as an estimate of soil age (Bockheim, 1980; McFadden, 1982; McFadden and Hendricks, 1985). Clay minerals form within a soil profile through in-situ chemical weathering of unstable minerals such as feldspars, micas, and hornblende. Over time, these clays along with clays from eolian sources continue to accumulate and form thick, progressively enriched argillic B-horizons.

Study Area and Previous Work

This study focuses on suite of soils developed on offset alluvial fan deposits of Little Rock Creek (LRC) between Palmdale and Valyermo in the Transverse Ranges of southern California (Figs. 1 and 2). The six Pleistocene-aged piedmont alluvial fans have been transported right laterally along the Mojave section of the San Andreas fault since deposition. The fans are numbered from 0 – 5 with increasing distance (0.68 – 16.50 km) from the original site of deposition at the outlet of LRC and range in age from 16 - 413 kyr. A probable slip rate of 3.0 ± 1.0 cm/yr has been calculated using the dates and offset distances of the LRC fans (Matmon et al., 2005) which agrees with previous studies of Quaternary slip rates of the Mojave section of the San Andreas fault.

The study area lies in transition between two ecoregions of the San Gabriel Mountains and the western Mojave Desert (Bailey et al., 1994). Mean annual precipitation ranges from 16.8 - 27 cm and mean annual temperature ranges from 12.1 - 17.2°C, measured from several Western Regional Climate Center stations between Palmdale, Pearblossom and Valyermo. Vegetation is composed of Joshua trees, creosote bush, California juniper and Mojave yucca.

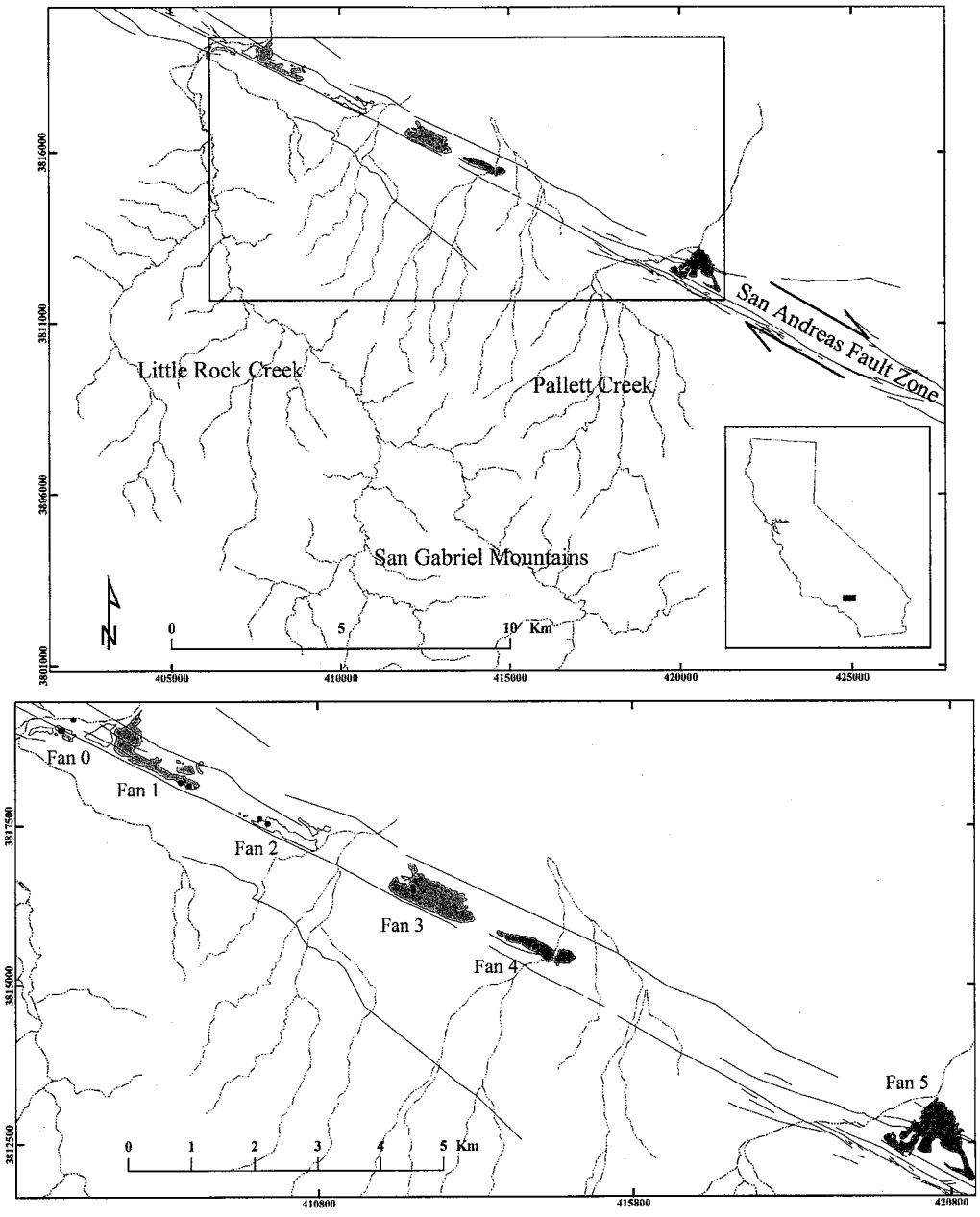

Figure 2. Location of study area in southern California along the San Andreas fault. The Little Rock Creek watershed is the largest drainage basin in the area at ~200 km^2. Circle symbols – location of soil profiles in this study (Appendix C; Table 7). A shutter ridge is found just NW of fan 0. Fan boundaries are modified from the geology of Barrows et al. (1985). Map datum is UTM, zone 11S, NAD27.

The morphologies of the preserved LRC fans are complex and appear to be partially controlled by the influence of an incised shutter ridge on the youngest fans (Fig. 2). Originally, LRC flowed north until its path was blocked by movement of a shutter ridge along the San Andreas fault. As LRC incised through the ridge, its outlet was constrained and offset with the gap. Because of this, Matmon et al. (2005) assumed that only the eastern side of the younger fans were preserved due to west side erosion of the fans by the continued shifting of the LRC channel gap from movement along the San Andreas fault. This is evident in numerous terraces preserved on the western margins of younger fans.

The surface morphologies of the fans, including relief and boulder densities, change with increasing age and distance offset from LRC (Matmon et al., 2005; Matmon et al., in press). Young fans (0-1) have the greatest surface relief and the highest boulder densities exposed on bar (topographic high) and swale (topographic low) surfaces. Progressively older fans (2-4) have less surface relief and low amounts of boulders exposed on bars with even less boulders found in swales. The oldest fan 5 has little surface relief and the least amount of boulders exposed on the surface. Matmon et al. (in press) proposed that as fan surfaces at LRC matured, boulders exposed on bars were eroded into grus and transported into swales. As bars were continually weathered and transported and filled in swales, the surface relief of the

fans decreased and resulting erosion rates decreased. Matmon et al. (in press) demonstrated this process by determining erosion rates calculated from cosmogenic nuclides on fans 2 - 5. The results show erosion rates decrease with increasing age and distance offset from LRC: fan 2, 48.4 ± 6.3 mm/kyr; fan 3, 41.2 ± 5.4 mm/kyr; fan 4, 27.7 ± 3.6 mm/kyr; and fan 5, 11.3 ± 1.5 mm/kyr.

Soil parent material is composed of weakly consolidated, well-rounded and sub-rounded cobbles and boulders up to 2 m long surrounded by grus in a sandy matrix. Boulders, cobbles, and gravels are composed mainly of granodiorite, quartz diorite, granite, and gneiss (Barrows et al., 1985; Matmon et al., 2005). Mafic boulders such as hornblende gabbro, hornblendite, and amphibolite are also found in lesser quantities. The source areas of the boulder lithologies are found in the San Gabriel Mountains outcropping south of the San Andreas fault within the LRC watershed (Barrows et al., 1985). Distinct lithologies such as the Lowe Granodiorite help distinguish alluvial fans derived from the LRC drainage basin from other major drainages along this section of the San Andreas fault.

Detailed mapping of the area conducted by Barrows et al. (1985) identified many of the gravel deposits north of the San Andreas fault, including the alluvial fans of LRC as one fan that was being offset during deposition based on differences in outcrop width on opposite sides of the San Andreas fault. However, Weldon et al.

(1993) had a different view about the fan formation and suggested each major drainage system from the San Gabriel Mountains deposited clasts of distinct assemblages on the western floor of the Mojave Desert, much like a conveyor belt system. Matmon et al. (2005) verified this hypothesis at LRC by calculating the ages of fans 0-1 and 3-5 using cosmogenic ^{26}Al and ^{10}Be (exposure and burial dating methods) and showed an increase in age of the LRC fans with increasing distance from the original site of deposition at LRC. The following ages of the LRC fans were calculated by Matmon et al. (2005): fan 0, 16 ± 5 ka; fan 1, 29 ± 7 ka; fan 3, 227 ± 242 ka; fan 4, 281 ± 181 ka; and fan 5, 413 ± 185 ka. Fan 2 was not dated due to possible surface modification from internal drainages formed on the fan surface after deposition.

FIELD AND LABORATORY PROCEDURES

A total of twelve soil pits were dug on fans 0 - 5 using a truck-mounted backhoe. Each fan surface included two soil profiles, one from a topographic high and one from a topographic low surface to account for the most extreme cases of soil variability. Soils formed on topographic high surfaces represent the most accurate record of soil development through time. Soils formed on topographic low surfaces represent cumulic or aggrading surfaces and vary in morphology when compared to topographic high soils (Harrison et al., 1990; Eppes and Harrison, 1999). Additional soil profile data were obtained from the active channel of LRC and fan 5 from a previous trenching study. Soil profiles were described and sampled using standard procedures (Birkeland, 1999). Soil color was determined by the Munsell soil color chart and particle size distribution was determined by dispersal of the <2 mm fraction in 10% sodium pyrophosphate, wet-sieve separation, and pipette extraction of the clay fraction from settling tubes. Bulk density was determined by the paraffin clod method (Singer, 1986).

Content and composition of pedogenic iron oxides, such as hematite and ferrihydrite was determined by selective chemical dissolution techniques (Appendix A). The concentrated citrate-dithionite method of Holmgren (1967) was used to determine total secondary iron oxyhydroxides (Fe_2O_3d). Poorly crystalline and

amorphous iron oxyhydroxides (Fe_2O_3o), such as ferrihydrite were extracted using the hydroxylamine procedure of Chao and Zhou (1983). Although acid ammonium oxalate (AAO) is a more commonly used method for determining Fe_2O_3o in soil chronosequences, several studies have found the hydroxylamine method to produce comparable results (Chao and Zhou, 1983; Ross et al., 1985; Lee et al., 1989). Additionally, magnetite does not need to be removed from the sample when using the hydroxylamine method and is more easily analyzed using atomic absorption than AAO. Citrate-dithionite and hydroxylamine extractable iron oxides were measured using an Instrumentation Laboratory Video 12 flame atomic absorption spectrometer (Appendix A). Profile mass (g/cm^2 soil column) of clay and iron oxides was determined (Appendix B) similar to the procedure used by McFadden and Hendricks (1985).

RESULTS

Soil Morphology and Clay content

The field descriptions of each soil are summarized in Table 2. Soils formed on topographic highs at LRC progress in development with increasing age and distance from LRC (Fig. 3). B-horizon thickness, clay percent of argillic horizons, and profile mass of clay increase with age (Table 2). Although fan 5 is the oldest soil, it shows a sharp decrease in B-horizon thickness (Table 2; Figs. 4, 5), clay content, and profile mass of clay. Soils formed on topographic lows are cumulic in nature as indicated by thick, fine grained nongravelly B-horizons developed over more gravelly parent material (Figs. 6, 7). The cumulic topographic low soils show greater profile mass of clay than soils from topographic high surfaces (Fig. 8). Calcium carbonate is not present in significant amounts at LRC. Also, profile LRC7 shows slight evidence of silica cementation of sand grains.

At LRC, profile mass of clay increases with ages on fans 0-4, while fan 5 shows a decrease in profile mass of clay (Fig. 8). Undated fan 2 shows greater clay and iron oxides than fan 1 and less than fan 3. In this study, topographic low fan surfaces initially accumulate profile mass of clay at a greater rate than topographic high surfaces. Rate of accumulation for profile mass of clay on topographic low soils best fits the logarithmic function, $Y = a + (b \log X)$, while soils formed on

topographic high surfaces best fit a power function, ln Y = a + (b ln X), where Y = profile mass of clay and X = time. Using the profile mass from dated fans 0-1, 3-4, the following equations are produced: for topographic lows, Y = - 14.74 + (7.23 log X), r^2 = 0.91; and for topographic highs, ln Y = - 0.79 + (0.72 log X), r^2 = 0.86 (Fig. 8).

Iron Oxide Analyses

Maximum weight percent and profile mass of Fe_2O_3d and Fe_2O_3o increase with soil age (Table 2; Fig. 9, 10). Initially on the topographic high surface of fan 0, the highest Fe_2O_3d weight percents are found in the A horizon, while the highest Fe_2O_3o is found in the upper C horizon (Table 2). In older soils, the maximum Fe_2O_3d percent values are found associated with maximum clay percent values found in Bw or upper Bt horizons. Greatest Fe_2O_3o horizon weight percent values increase from 0.2 at fan 0, to a maximum of 1.68 at fan 3, then decrease to 0.40 – 0.53 at fan 5. In this study, soils at LRC initially accumulate Fe_2O_3d rapidly, but with time slow in the rate of accumulation (Fig. 9). This contributes to the increasing ratio of profile clay verses Fe_2O_3d with time and shows the decrease in the rate of iron oxide accumulation (Fig. 11).

Table 2. Summary of Soil Properties and Lab Results in the Little Rock Creek Soil Chronosequence

Soil Profile	Fan	Age[a] (ka)	Sample Number	Profile Horizon[b]	Depth (cm)	Color Dry[c]	Structure[d]	Consistence[e]	wet[f]	Texture[g]	Total Gravels[h] (%)	Particle size, <2 mm Sand (%)	Silt (%)	Clay (%)	Fe_2O_3d (%)	Fe_2O_3o (%)	Fe_2O_3o/ Fe_2O_3d ratio	Profile Mass (g/cm²) Clay	Fe_2O_3d	Fe_2O_3o
LRC14	active wash		LRC97	AC	0-5	2.5Y 7/2	sg	lo / lo	so / po	S	27	93.96	5.51	0.53	0.61	0.16	0.27	0.03	0.03	0.01
			LRC98	C(1)	5-10		sg	lo / lo	so / po	S	15	97.24	1.76	1.00	0.68	0.18	0.26			
			LRC99	C(2)	10-15	2.5Y 6/3	sg	lo / lo	so / po	S	15	97.12	2.59	0.29	0.60	0.18	0.30			
			LRC100	C(3)	15-20	2.5Y 6/2	sg	lo / lo	so / po	S	15	97.09	2.41	0.50	0.77	0.19	0.24			
			LRC101	C(4)	20-25		sg	lo / lo	so / po	S	30	96.88	2.38	0.74	0.58	0.21	0.35			
			LRC102	C(5)	25-30		sg	lo / lo	so / po	S	56	96.21	2.67	1.12	0.53	0.19	0.35			
			LRC103	C(6)	30-35		sg	lo / lo	so / po	S	53	91.80	6.90	1.31	0.71	0.28	0.39			
			LRC104	C(7)	35-40	2.5Y 5/3	sg	lo / lo	so / po	LS	28	86.32	9.27	4.41	0.73	0.31	0.42			
LRC1	0	16±5	LRC1	A	0-12	10YR 5/3	1bmpl	sh / vfr	so / po	SL	15	73.94	21.95	4.10	0.93	0.19	0.20	2.56	0.47	0.12
			LRC2	Bw1	12-30	10YR 6/4	2msbk	sh / vfr	so / po	LS	60	76.38	18.24	5.38	0.77	0.18	0.24			
			LRC3	Bw2	30-64	10YR 6/2	3msbk	so / vfr	so / po	LS	33	83.28	13.03	3.69	0.68	0.19	0.28			
			LRC4	C(1)	64-80	10YR 7/1	m	lo / lo	so / po	S	51	90.17	8.15	1.68	0.57	0.20	0.36			
			LRC5	C(2)	80-100					S	51	90.76	5.18	4.07	0.57	0.16	0.28			
LRC2	0	16±5	LRC6	A	0-7	2.5Y 6/3	1bmpl	sh / vfr	ss / po	SL	15	75.52	16.85	7.63	0.67	0.17	0.26	1.97	0.21	0.08
			LRC7	Bw	7-20	2.5Y 5/3	3sbk	h / fr	ss / po	SL	10	76.74	16.50	6.77	0.77	0.35	0.46			
			LRC8	2C1	20-40	2.5 6/3	m	vh / fi	so / po	SL	5	76.91	15.38	7.71	0.68	0.26	0.37			
			LRC9	3C2	40-45	2.5Y 6/2	msg	lo / lo	so / po	S	3	93.22	4.82	1.96	1.06	0.15	0.14			
LRC3	1	29±7	LRC10	A	0-5	10YR 5/4	3fpl	sh / vfr	ss / sp	SL	22	74.21	20.33	5.46	0.96	0.20	0.21	7.53	1.19	0.65
			LRC11	Bw1	5-23	10YR 5/4	3msbk	sh / vfr	ss / po	SL	12	75.43	17.94	6.63	1.01	0.20	0.19			
			LRC12	Bw2(1)	23-50	10YR 5/4	2fsbk	sh / vfr	so / po	SL	25	74.33	18.72	6.95	0.96	0.31	0.32			
			LRC13	Bw2(2)	50-65					LS	25	78.82	15.87	5.31	0.83	0.70	0.84			
			LRC14	Bw2(3)	65-88					LS	5	76.62	19.15	4.22	0.84	0.91	1.09			
			LRC15	2Bwb	88-98	10YR 6/4	3fsbk	vh / fr	ss / ps	SL	5	71.82	22.65	5.53	0.80	0.31	0.39			
			LRC16	2C	98-118	7.5YR 7/4	m	vh / fr	so / po	LS	5	80.62	16.64	2.74	1.05	0.16	0.15			
LRC4	1	29±7	LRC17	A	0-10	2.5YR7/3	3mpl	sh / vfr	ss / ps	SCL	3	66.02	24.41	9.57	1.03	0.14	0.14	13.68	1.27	0.21
			LRC18	Bw1	10-35	10YR 6/4	3msbk	sh / vfr	ss / ps	SL	2	76.09	16.09	7.82	1.05	0.14	0.13			
			LRC19	Bw2(1)	35-55	10YR 5/4	m	h / fr	ss / ps	SCL	2	64.83	21.62	13.54	1.13	0.23	0.21			
			LRC20	Bw2(2)	55-80					SL	2	66.52	19.33	14.14	1.02	0.19	0.19			
			LRC21	C(1)	80-100	2.5Y 6/4	m	h / fr	ss / ps	SC	0	60.87	36.01	3.12	0.96	0.22	0.23			
			LRC22	C(2)	100-130					SCL	0	60.83	31.58	7.59	0.96	0.24	0.25			
			LRC23	C(3)	130-160					SCL	0	63.26	21.66	15.08	0.94	0.25	0.26			
			LRC24	C(4)	160-200					SCL	0	67.76	21.31	10.92	1.02	0.20	0.19			
LRC5	2	no date	LRC25	A	0-12	10YR 5/4	2mpl	sh / vfr	so / ps	LS	38	77.12	17.85	5.03	0.95	0.23	0.25	10.40	1.16	0.82
			LRC26	Bt	12-37	10YR 4/4	3msbk	h / fr	so / ps	SL	28	71.85	14.74	13.41	1.24	0.56	0.46			
			LRC27	Bw1(1)	37-50	10YR 5/4	3msbk	sh / fr	ss / ps	SL	25	76.94	12.78	10.28	1.14	0.85	0.75			
			LRC28	Bw1(2)	50-65					LS	25	82.85	8.93	8.22	0.96	0.76	0.78			
			LRC29	Bw2(1)	65-80	10YR 6/4	m	sh / vfr	ss / ps	SL	40	80.61	11.49	7.89	0.89	0.95	1.06			
			LRC30	Bw2(2)	80-100					SL	40	81.71	12.02	6.25	0.83	0.91	1.10			
			LRC31	Cox	100-145	2.5Y 6/4	m	sh / vfr	so / po	LS	75	87.96	8.88	3.15	0.80	0.88	1.10			
			LRC32	Cox	145-160	2.5Y 7/4	m	lo / lo	so / po	S	55	92.13	4.95	2.91	0.84	0.55	0.65			
LRC6	2	no date	LRC33	A	0-15	10YR 6/4	3fpl	sh / vfr	so / po	SL	15	81.80	14.08	4.11	0.72	0.16	0.22	9.06	1.69	0.56
			LRC34	Bw1	15-30	10YR 6/4	3msbk	sh / vfr	so / po	SCL	10	74.45	23.48	2.07	1.04	0.23	0.22			
			LRC35	Bw2(1)	30-50	10YR 7/6	3msbk	sh / vfr	so / po	SCL	20	70.43	22.44	7.13	1.17	0.34	0.29			
			LRC36	Bw2(2)	50-80					SCL	20	73.13	21.04	5.83	1.06	0.39	0.37			
			LRC37	Bw3	80-115	10YR 8/6	m	sh / vfr	so / po	SCL	25	71.97	23.04	4.99	0.80	0.33	0.41			
			LRC38	Cox(1)	115-140	10YR 8/4	m	sh / vfr	so / po	SCL	25	69.37	26.71	3.92	0.70	0.30	0.43			
			LRC39	Cox(2)	140-170	10YR 8/4	m	sh / vfr	so / po	SCL	15	69.44	26.21	4.35	0.64	0.28	0.44			
LRC7	3	227±242	LRC40	A	0-8	10YR 5/3	2mgr	sh / vfr	so / po	SL	26	74.81	17.20	7.98	1.03	0.25	0.24	14.50	1.67	1.52
			LRC41	AB	8-14	10YR 4/4	1fsbk->2mgr	sh / fr	so / po	SL	31	71.15	19.80	9.00	1.11	0.26	0.23			
			LRC42	Bt1(1)	14-35	7.5YR 4/4	2fsbk	h / fr	ss / ps	SL	46	63.98	17.50	18.50	1.38	0.54	0.39			
			LRC43	Bt1(2)	35-50					SL	46	61.71	20.74	17.53	1.42	1.68	1.19			
			LRC44	Bt2(1)	50-70	10YR 5/6	1fsbk->m	sh / fr	so / po	SL	46	68.22	19.85	11.91	1.13	1.27	1.12			
			LRC45	Bt2(2)	70-95					SL	46	77.04	15.49	7.46	1.19	1.30	1.09			
			LRC46	2BC	95-135	2.5YR 6/3	sg	sh / fr	so / po	LS	37	80.53	13.13	6.32	1.13	1.21	1.07			
			LRC47	3C	135-153	2.5YR 6/3	m	lo / lo	so / po	S	48	87.95	8.37	3.67	0.99	0.42	0.43			
			LRC48	4C	153-180	2.5YR 5/4	sg	lo / lo	so / po	LS	88	84.16	11.92	3.91	0.98	0.49	0.49			
LRC8	3	227±242	LRC49	A	0-5	10YR 5/3	2mgr	so / vfr	so/ po	SCL	10	60.78	33.63	5.59	0.70	0.13	0.19	25.61	2.42	0.55
			LRC50	BA	5-14	10YR 5/4	1msbk	sh / fr	so / ps	SCL	10	60.57	32.96	6.47	0.97	0.15	0.16			
			LRC51	Bw1(1)	14-30	10YR 5/4	2m-csbk	h / fr	so / ps	SCL	15	60.76	31.97	7.27	0.84	0.14	0.16			
			LRC52	Bw1(2)	30-60					SCL	15	61.28	29.78	8.95	0.95	0.16	0.17			
			LRC53	Bw1(3)	60-90					SCL	15	56.19	29.74	14.06	0.89	0.19	0.21			
			LRC54	Bw1(4)	90-110					SCL	15	59.28	30.61	10.11	1.02	0.27	0.27			
			LRC55	Bw2	110-140	10YR 5/4	1msk->m	h / fr	so / ps	SCL	10	62.98	25.53	11.49	1.14	0.31	0.27			
			LRC56	2Bw	140-170	10YR 5/4	1msk->m	sh / fr	so / po	SCL	32	62.11	25.24	12.65	1.16	0.28	0.24			
			LRC57	2Bt	170-200	7.5YR 5/4	1msk->m	h / fr	ss / ps	SCL	49	65.35	22.97	11.68	1.16	0.29	0.25			

Table 2 Continued. Summary of Soil Properties and Lab Results in the Little Rock Creek Soil Chronosequence

Soil Profile	Fan	Age[a] (ka)	Sample Number	Profile Horizon[b]	Depth (cm)	Color Dry[c]	Structure[d]	Consistence[e]	wet[f]	Texture[g]	Total Gravels[h] (%)	Particle size, <2 mm Sand (%)	Silt (%)	Clay (%)	Fe_2O_3d (%)	Fe_2O_3o (%)	Fe_2O_3o/ Fe_2O_3d ratio	Profile Mass (g/cm²) Clay	Fe_2O_3d	Fe_2O_3o
LRC9	4	281±181	LRC58	A	0-10	10YR 5/4	1fsbk->2mgr	sh / vfr	so / po	SCL	0	70.68	26.22	3.09	0.96	0.18	0.18	39.16	2.53	0.94
			LRC59	AB	10-22	10YR 5/4	1mgr	sh / vfr	so / po	SCL	7	70.00	22.12	7.87	1.07	0.24	0.23			
			LRC60	Bt1(1)	22-50	7.5YR 4/6	3c/mpr	vh / vf	ss / ps	SL	10	58.11	18.30	23.57	1.32	0.39	0.30			
			LRC61	Bt1(2)	50-72					SL	10	64.15	15.16	20.69	1.18	0.57	0.48			
			LRC62	Bt2(1)	72-100	10YR 5/6	1f/msbk->m	h / fi	ss / ps	SL	35	62.19	14.43	23.37	1.24	0.57	0.46			
			LRC63	Bt2(2)	100-135					SL	41	64.08	15.78	20.13	1.22	0.46	0.38			
			LRC64	BC	135-165	10YR 5/6	1f/msbk->m	h / fi	ss / ps	SCL	68	65.04	22.18	12.18	1.08	0.43	0.40			
			LRC65	C	165 +	10 YR 5/4	m	sh / vfr	so / po	SL		77.47	15.37	7.16	0.98	0.39	0.39			
LRC10	4	281±181	LRC66	A	0-9	10YR 5/4	1tnpl->2mgr	s / vfr	so / po	LS	10	83.20	12.93	3.87	0.79	0.12	0.15	24.08	3.18	0.72
			LRC67	AB	9-17	10YR 5/4	2mgr->m	sh / vfr	so / po	SL	5	80.10	14.37	5.52	0.97	0.15	0.15			
			LRC68	Bw(1)	17-50	10YR 4/4	1m/csbk	mh / fr	ss / po	SL	8	69.94	19.59	10.47	1.15	0.21	0.19			
			LRC69	Bw(2)	50-85					SCL	8	71.96	21.47	6.57	1.13	0.24	0.21			
			LRC70	BC(1)	85-100	10YR 5/4	1msbk	sh / vfr	so / po	SL	10	72.59	19.79	7.63	1.07	0.29	0.27			
			LRC71	BC(2)	100-114					SCL	10	72.59	20.99	6.42	1.07	0.30	0.28			
			LRC72	2Bw	114-145	10YR 5/4	1msbk	sh / vfr	so / po	SL	12	74.25	17.62	8.13	1.01	0.29	0.28			
			LRC73	2Bt	145-200	10YR 5/4	1f/msbk	h / fr	so / po	SL	15	72.81	17.78	9.41	1.09	0.24	0.22			
LRC11	5	413±185	LRC74	A	0-12	10YR 5/4	2tnpl->1fsbk	s / vfr	so / po	SCL	26	62.37	33.70	3.92	1.05	0.23	0.22	7.79	0.87	0.30
			LRC75	BA(1)	12-25	10YR 5/4	1msbk	sh / vfr	so / po	SCL	87	71.68	21.39	6.93	1.08	0.24	0.22			
			LRC76	BA(2)	25-39					SCL	82	66.32	21.73	11.94	1.16	0.37	0.32			
			LRC77	Bw	39-68	10YR 5/3	2f/msbk	sh / fr	so / ps	SCL	52	66.88	21.16	11.95	1.21	0.43	0.36			
			LRC78	Bt1(1)	68-85	10YR 5/4	1msbk	h / fr	ss / ps	SCL	62	63.57	21.22	15.19	1.34	0.51	0.38			
			LRC79	Bt1(2)	85-102					SL	62	71.00	17.41	11.60	1.26	0.51	0.40			
			LRC80	Bt2	102-123	10YR 4/6	1msbk	h / fr	ss / ps	SL	77	71.33	17.85	10.80	1.12	0.43	0.39			
			LRC81	C	123-150	10YR 5/4	m	sh / vfr	ss / ps	SL	77	76.85	7.36	15.79	1.03	0.33	0.32			
LRC12	5	413±185	LRC82	A	0-14	10YR 4/3	1fsbk->2mgr	s / vfr	so / po	SL	12	79.89	17.99	2.12	0.85	0.13	0.16	13.44	3.16	0.78
			LRC83	Bw(1)	14-30	10YR 5/4	2csbk->2f/msbk	sh / vfr	so / po	SL	7	77.11	18.45	4.44	1.05	0.19	0.18			
			LRC84	Bw(2)	30-50					SL	7	78.11	17.84	4.04	1.07	0.19	0.18			
			LRC85	Bw(3)	50-70					SCL	7	77.73	21.73	0.54	1.09	0.21	0.19			
			LRC86	Bw(4)	70-90					SCL	7	78.19	20.09	1.73	1.03	0.21	0.20			
			LRC87	Bw(5)	90-110					SL	7	78.17	15.56	6.27	1.09	0.24	0.22			
			LRC88	Bw(6)	110-140					SL	7	76.15	17.35	6.50	1.10	0.28	0.26			
			LRC89	BC(1)	140-170	10YR 5/4	1msbk->m	sh / fr	so / po	SL	5	71.52	19.33	9.15	1.20	0.41	0.34			
			LRC90	BC(2)	170-200					SCL	5	74.00	22.82	3.18	1.19	0.37	0.31			
LRC13[j]	5	413±185	LRC91	A	0-22	10YR 3/3			so / ps	SCL		70.42	20.84	8.74	1.33	0.21	0.16			
			LRC92	AB	22-50	10YR 4/6			so / ps	SCL		65.82	21.42	12.76	1.39	0.36	0.26			
			LRC93		50-80	10YR 4/6			so / ps	SCL		63.20	21.57	15.23	1.41	0.53	0.37			
			LRC94		80-110	10YR 4/6			so / po	SL		71.23	18.05	10.72	1.39	0.39	0.28			
			LRC95		110-170	10YR 5/4			so / po	LS		82.10	8.47	9.43	1.07	0.22	0.20			
			LRC96		170-200	10 YR 5/4			so / po	LS		83.33	4.20	12.47	1.21	0.28	0.23			

[a] Fan ages from Matmon et al. (2005)

[b] Numbers in parenthesis represent subdivsions of a horizon used for laboratory analysis

[c] Dry color from the Munsell Soil Color chart

[d] m = massive, sg = single grain, 1 = weak, 2 = moderate, 3= strong; vf = very fine, f = fine, m = medium, c = coarse; gr = granular, sbk = subangular blocky, pl = platy, pr = prismatic; -> = parting to

[e] lo = loose, so = soft, sh = slighly hard, h = hard, vh = very hard; lo = loose, vfr = very friable, fr = friable,fi = firm

[f] so = nonsticky, ss = slightly stickly, s = sticky, vs = very sticky; po = nonplastic, ps = slightly plastic, p = plastic, vp = very plastic

[g] S = sand, Si = silt, C = clay, L = loam

[h] Total gravel percents was visually estimated in the field of gravels, stones, and cobbles

[i] Profile mass content calculated similarly to McFadden McFadden and Hendricks (1985)

[j] Limited soil data available for profile

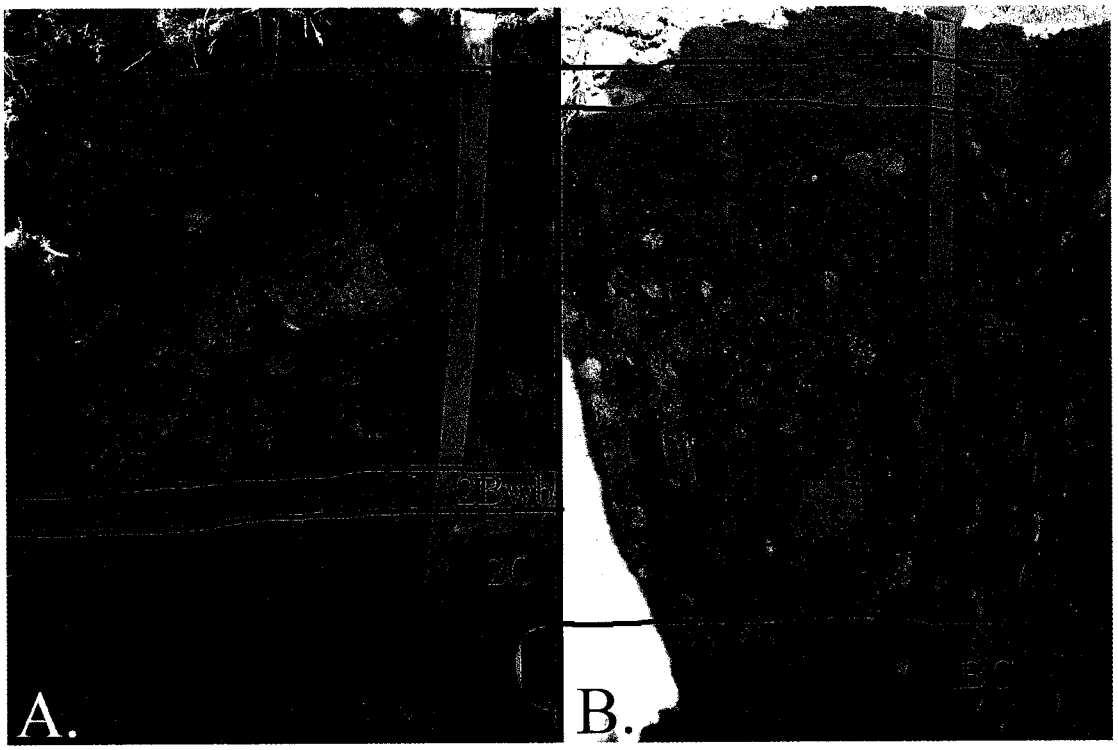

Figure 3. Soil development on topographic high surfaces. (A) Soil profile LRC 1 on fan 1 (29 ± 7 ka). (B) Soil profile LRC9 on fan 4 (281 ± 181 ka). Notice the differences between the soils of different ages. LRC 1 has a Bw-horizon, unweathered clasts while LRC9 has a thick well-developed argillic B-horizon, weathered clasts, and soil reddening due to iron oxide accumulation. Length of measuring tape is 1.4 m.

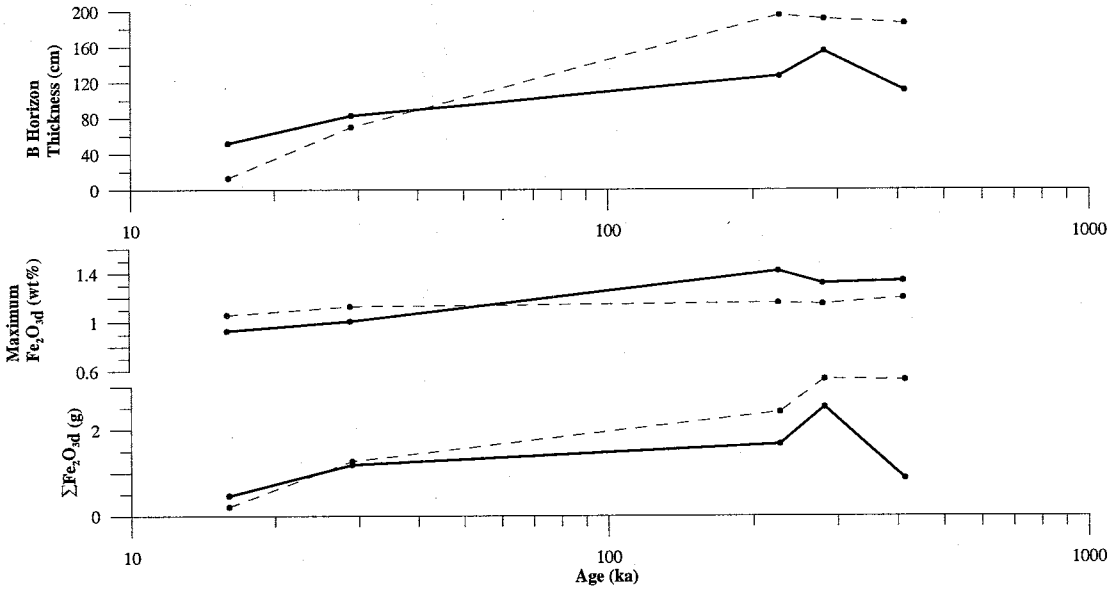

Figure 4. B-horizon thickness, maximum Fe_2O_3d percent, and profile mass Fe_2O_3d with increasing (log) age for dated fans at LRC. Solid lines are topographic high profiles and dashed lines are topographic low profiles.

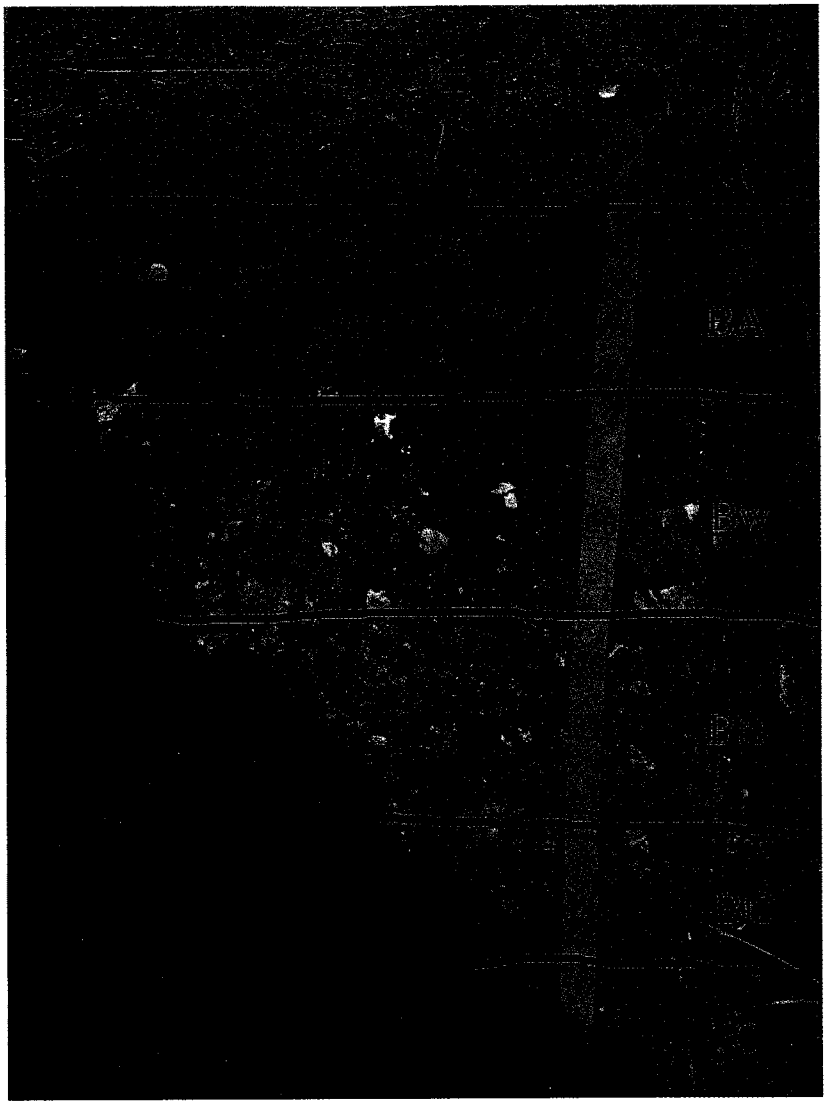

Figure 5. Topographic high soil profile LRC 11 from fan 5. Notice the lack of a fine-grained B-horizon. Length of measuring tape is 1.4 m.

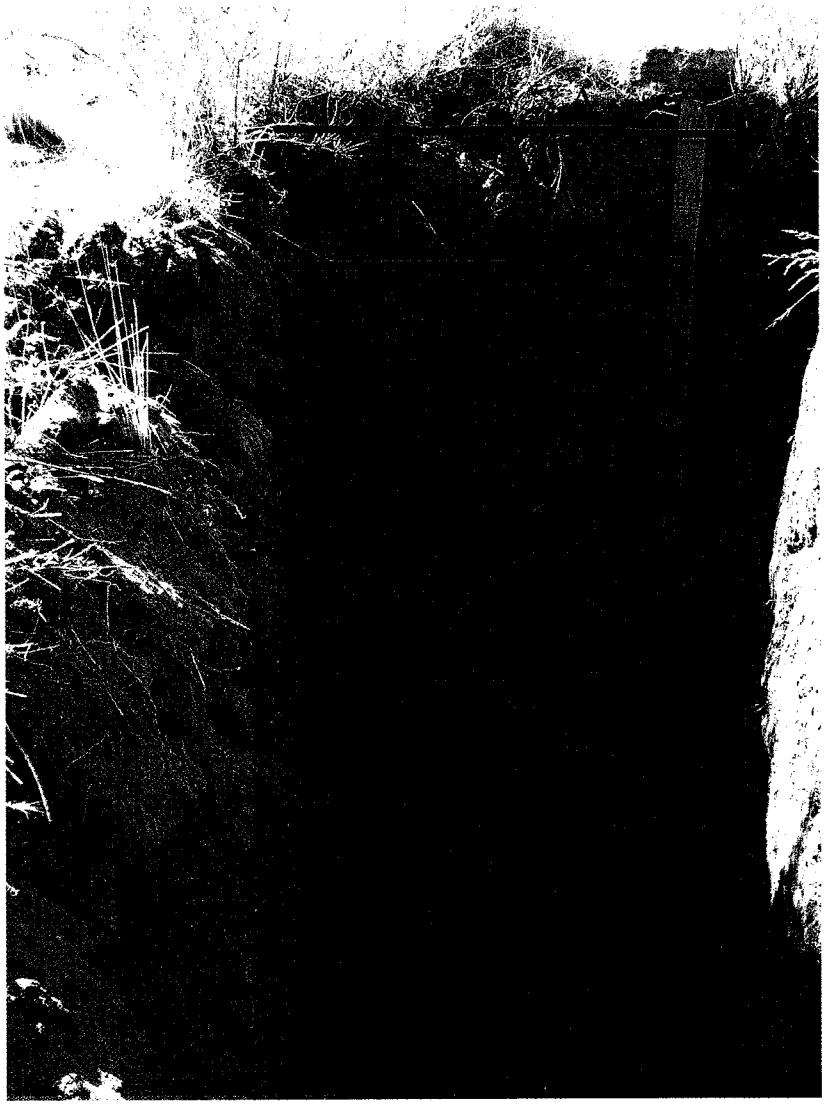

Figure 6. Example of a fine-grained topographic low soil (LRC 8) from fan 3. Length of measuring tape is 1.4 m.

Figure 7. Example of soil development with increasing age on topographic low soils, (A) Fan 2 topographic low soil LRC6 (no age). (B) Fan 5 topographic low soil LRC 12 (413 ± 185 ka). Notice the reddening of the profile with increasing age from the accumulation of iron oxides. Length of measuring tape is 1.4 m.

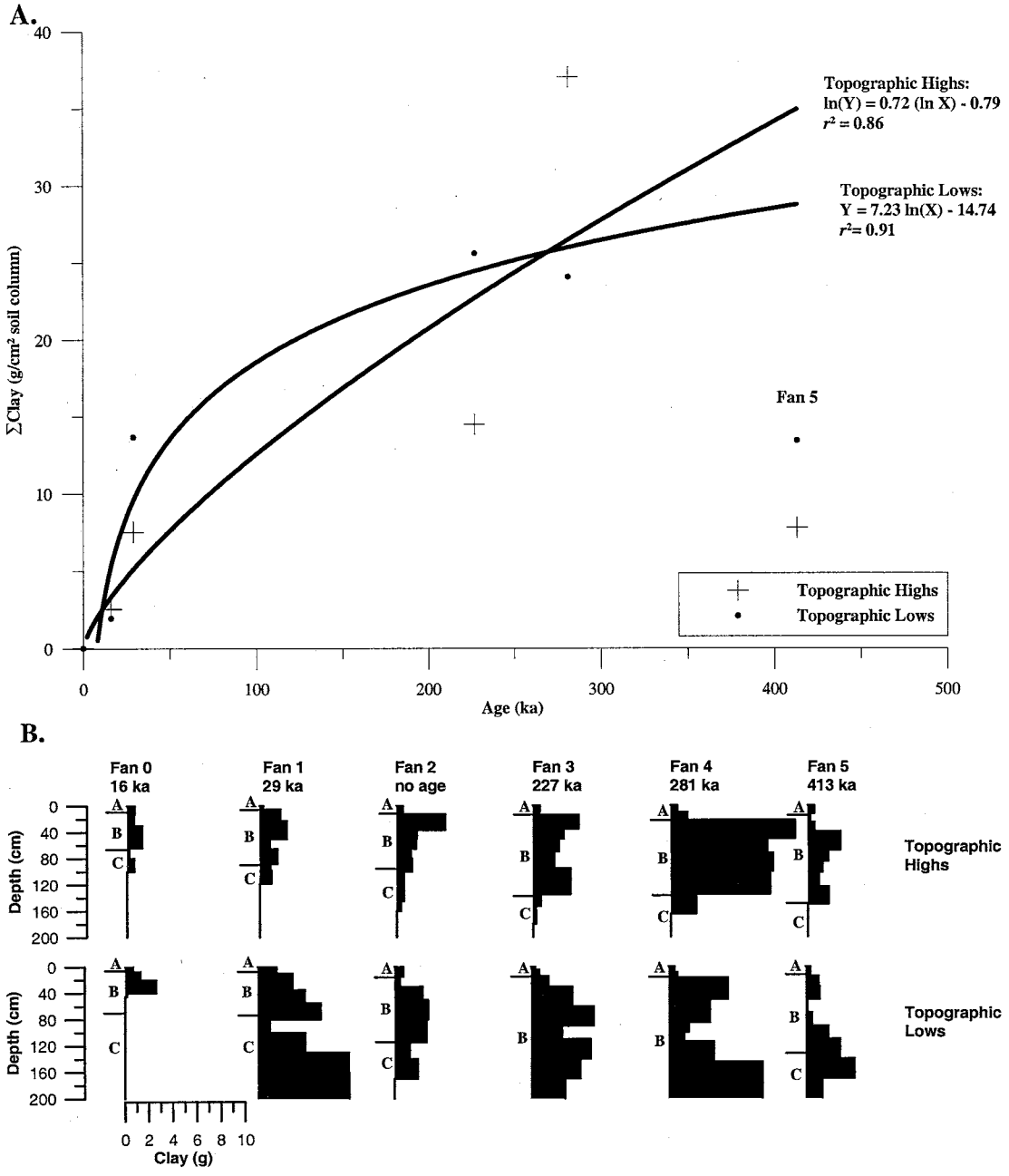

Figure 8. Changes in profile mass of clay for topographic highs and lows. (A) Profile mass of clay with increasing ages and resulting chronofunctions using dated fans 0, 1, 3, 4. Fan 5 was not used in the calculation of chronofunctions because of significant erosion. (B) Profile mass of clay with increasing depth for all fans. Notice the marked decrease of profile mass for fan 5.

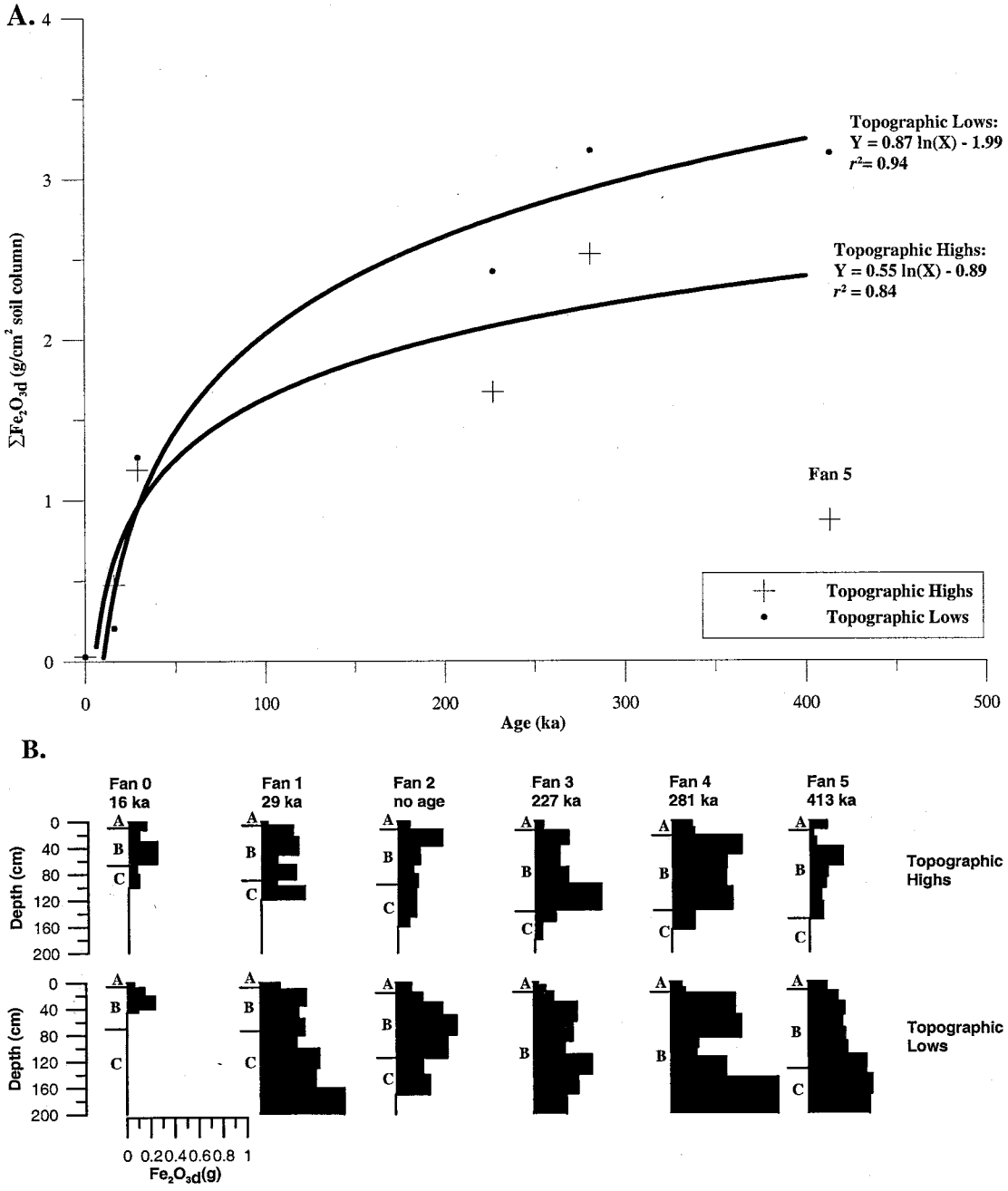

Figure 9. Changes in profile mass of Fe_2O_3d for topographic highs and lows. (A) Profile mass of Fe_2O_3d with increasing ages and resulting chronofunctions using dated fans 0, 1, 3, 4. Fan 5 was not used in the calculation of chronofunctions because of increased erosion. (B) Profile mass of Fe_2O_3d with increasing depth for all fans. Notice the marked decrease of profile mass for fan 5.

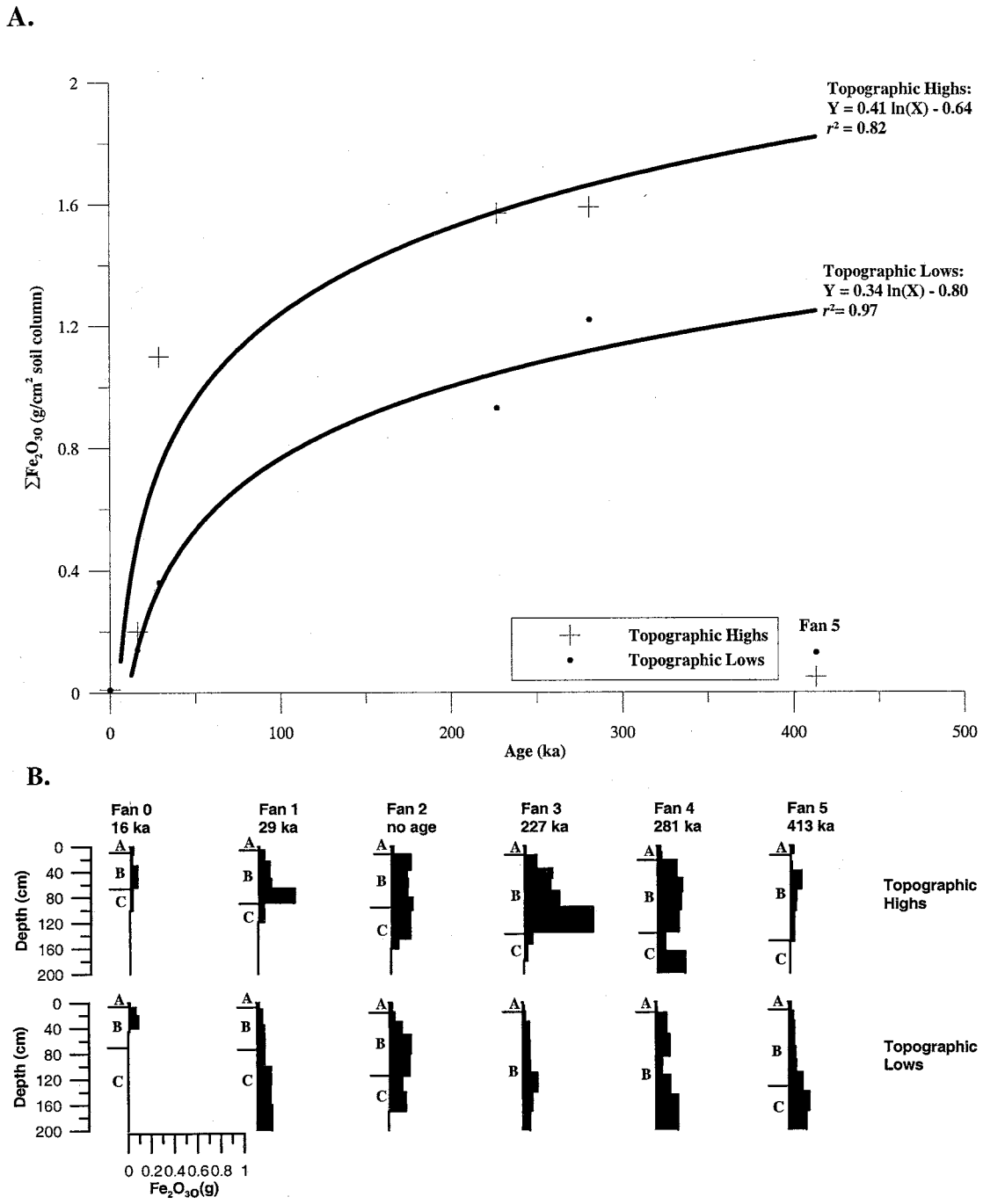

Figure 10. Changes in profile mass of Fe_2O_3o for topographic highs and lows. (A) Profile mass of Fe_2O_3o with increasing ages and resulting chronofunctions using dated fans 0, 1, 3, 4. (B) Profile mass of Fe_2O_3o with increasing depth for all fans. Notice the marked decrease of profile mass for fan 5.

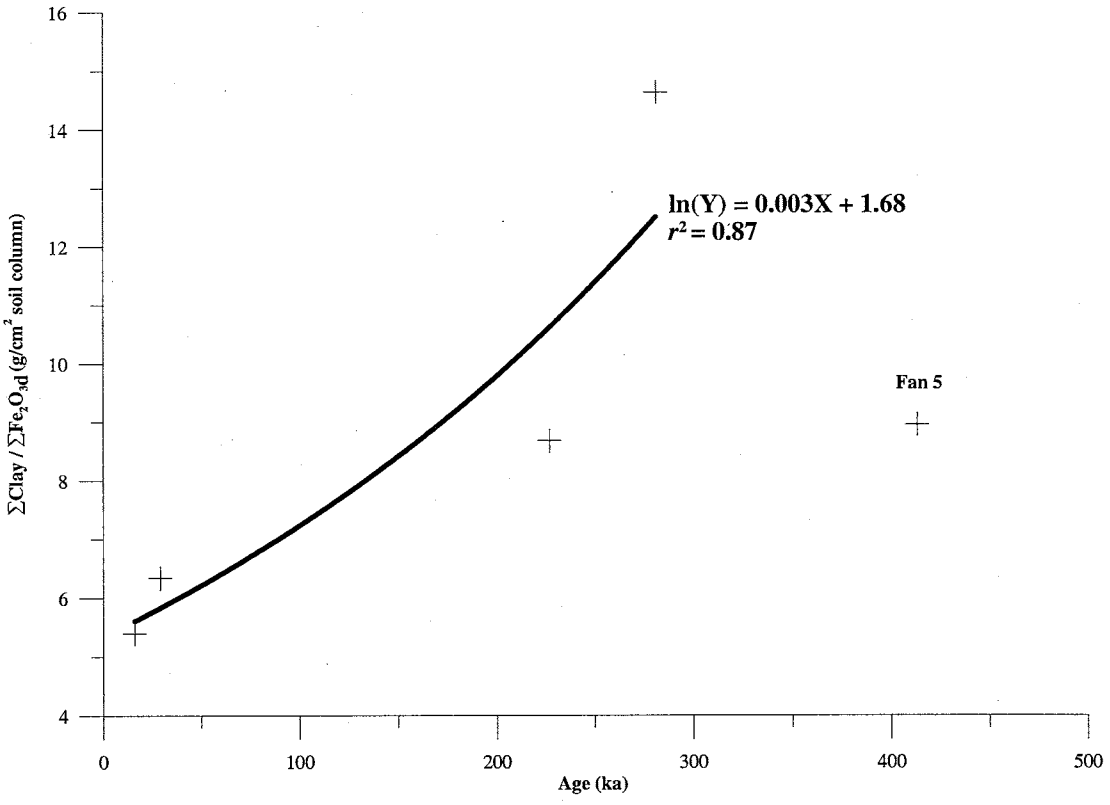

Figure 11. Relation between the ratio of profile clay verses Fe_2O_3d with time for topographic high surfaces. Fan 5 data were not used in the creation of the curve because of substantial erosion.

Previous studies have also shown strong linear relationship between Fe_2O_3d and clay content in soils since both are products of weathering in soils (McFadden, 1982; McFadden and Hendricks, 1985). Figure 12 shows the relationship between profile mass of clay and Fe_2O_3d for topographic highs and lows at LRC. Based on the graph, topographic high soils show a stronger linear relationship between profile clay and Fe_2O_3d than corresponding topographic lows. Rate of accumulation of Fe_2O_3d at LRC best fits the logarithmic function, $Y = a + (b \log X)$, where Y = profile mass of Fe_2O_3d and X = time. Using profile masses of Fe_2O_3d for dated fans 0-1, 3-4, the following equations are produced for topographic highs, $Y = -0.89 + (0.55 \log X)$, $r^2 = 0.84$; and topographic lows, $Y = -1.99 + (0.87 \log X)$, $r^2 = 0.94$ (Fig. 9). Fan 5 was not used in calculation of functions because the low profile mass of Fe_2O_3d shows evidence of significant erosion which will be addressed in the discussion section. Fe_2O_3o accumulates logarithmically similarly to Fe_2O_3d at LRC following the equations: $Y = -0.64 + (0.41 \ln X)$, $r^2 = 0.82$, for topographic highs; and topographic lows, $Y = -0.80 + (0.34 \ln X)$, $r^2 = 0.97$ (Fig. 10).

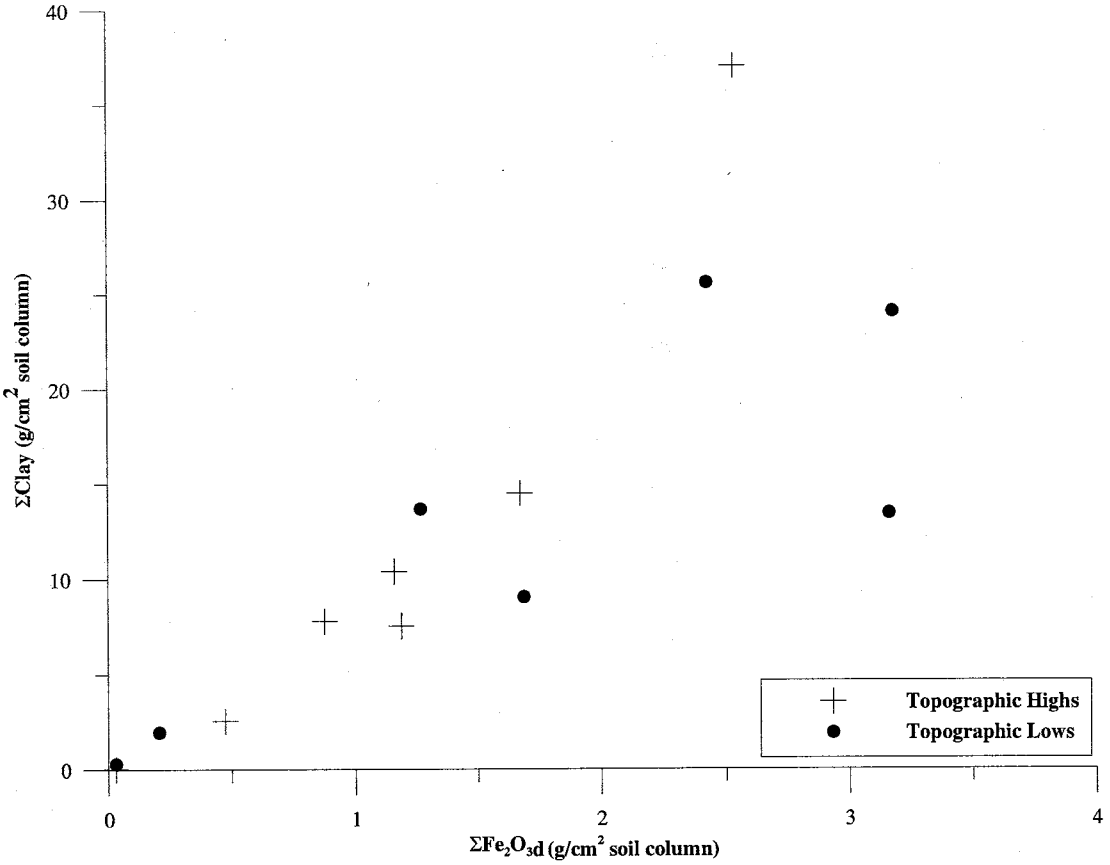

Figure 12. Relationship between profile mass of clay verses Fe_2O_3d for topographic high and low soil profiles.

DISCUSSION

The soils in this study show evidence of increasing development with increasing age and distance from LRC. The development and increasing thickness of argillic horizons, increases in weight percent and profile mass of clay and iron oxides show continued development with time, with the exception of fan 5.

Initially the rate of accumulation of clay on topographic low surfaces is rapid and decreases with time. This may reflect the changing geometry of a topographic low's catchment area. Early conditions favor rapid accumulation of material that is focused into a small surface area. As a depression fills, the surface area increases and material is accumulated over a larger surface area, which results in a lower rate of accumulation (Eppes, 1996). Topographic low surfaces also show greater soil variability, profile mass of clay, iron oxides, B-horizon thickness, and lower gravel percents than corresponding topographic high surfaces (Table 2; Figs. 9, 10, 11). This suggests topographic low soils are cumulic or aggrading surfaces and inherit clay and iron oxides from the erosion of surrounding topographic high areas. As surfaces erode from multiple topographic high surfaces to lows, complex contributing area geometries may change the resulting soil variability. The absence of buried soils and thick, weakly developed fine-grained B-horizons found in topographic lows show the continual rather than episodic infilling of topographic lows with fine-grained

sediments from surface runoff (Table 2). Figure 12 shows the differences in variability in the accumulation of profile mass of clay and Fe_2O_3d on topographic high and corresponding low surfaces. The topographic high profiles show that as profile mass of clay increases, so does Fe_2O_3d. However, on topographic low surfaces, the correlation between clay and Fe_2O_3d is much more variable. Harrison et al. (1990) found variation in soil properties between bar and swale sites formed on the same geomorphic surface. This was due to differences in the rate of eolian accumulation and surface runoff differences between bar and swale sites. Figures 9, 10, 11 also show soil variability between topographic high and low soils. The bimodal distribution of clay and iron oxides within topographic low soils may result from the eroding and subsequent deposition of argillic horizons from topographic high profiles. This might also explain why topographic low C-horizons have higher initial clay and iron oxide masses than corresponding topographic high profiles.

The increase of iron oxide (Fe_2O_3d and Fe_2O_3o) percent and profile mass with increasing soil age demonstrates the ongoing hydrolytic weathering of unstable mafic minerals from ferrous (Fe^{+2}) to ferric (Fe^{+3}) iron. At LRC, the soils accumulate pedogenic iron oxides most rapidly early in their development and with time, the accumulation rate decreases. McFadden and Hendricks (1985) offered several reasons for initially rapid weathering rates of ferrous iron that decrease with time: (1) fresh

mineral faces are exposed to CO_2-rich oxidizing soil moisture that supports rapid dissolution, but with time minerals become coated in clay, iron oxides and organic matter that decrease the rate of weathering, (2) as clay accumulates and decreases the infiltration and increases the water holding capacity, mineral-solution equilbria may be approached, which supports decreased rate of iron oxide accumulation, and (3) the depletion of unstable mafic minerals may decrease the rate of iron oxide accumulation. Yaalon (1971) also sited poorer drainage conditions through the continued incorporation of clay, resulting in the shift from conditions favoring oxidizing to more reducing soil environment that would decrease the rate of Fe_2O_3d formation.

Soils at LRC accumulate iron oxides with time like other southern California soil chronosequence studies (McFadden, 1982; McFadden and Hendricks, 1985; McFadden and Weldon, 1987; Kendrick and McFadden, 1996), however, at a lower rate. This could be due to climate and eolian flux differences between the studies. LRC has lower annual precipitation (17-27 cm) than Cajon Pass, 60 cm or the San Timoteo Badlands (36 cm) (McFadden and Hendricks, 1985; Kendrick and McFadden, 1996). Additionally, LRC has a slightly cooler temperature of 12-17.2°C than the ~17°C of other studies. McFadden and Hendricks (1985) suggested a drier

and cooler climate would lead to relative reduced rates of leaching and chemical alteration resulting in lower secondary iron oxide accumulations.

LRC soils also have less of an eolian input than other regional chronosequences based on location from a dust source, wind directions, and soil geomorphology. The Cajon Pass chronosequence has a significant dust source and is located in a wind gap, whereas LRC is not located downwind from a large dust source such as the Mojave Desert and prevailing wind directions in the region are to east and southeast away from the Mojave Desert (Reheis et al., 1995). Also, soil profiles at LRC lack Av horizons and high silt contents near the surface. Additionally, many profiles contain less silt than parent material values (Table 2). McFadden and Weldon (1987) found a linear correlation ($r^2 = 0.83$) between Fe_2O_3d and silt percent in Holocene soils in the Cajon Pass chronosequence suggesting eolian sources for silt content and Fe_2O_3d. At LRC, however, there is not a correlation ($r^2 = 0.0004$) between Fe_2O_3d and silt percents in soil horizons suggesting a non eolian source of silts. Many studies have shown the importance of dust as a source of calcium carbonate in soils in arid regions (Wells et al., 1987; Reheis et al., 1995). If LRC soil development was significantly affected by calcareous dust, it should be present in the soil profiles. However, soils at LRC are not reactive to HCl and do not appear to accumulate calcium carbonate ($CaCO_3$).

Soil Morphology of Fan 5

There are several possible reasons for low amount of soil development on fan 5. These could include: formation of post-depositional drainages, modification from nearby Pallet Creek, and a crossing of a pedogenic threshold. The decrease in B-horizon thickness and profile masses of clay and Fe_2O_3d suggests the topographic high surface of fan 5 has been significantly modified or stripped since deposition. Fan 5 is the oldest in the sequence of fans at LRC and theoretically should have the most developed soils with the thickest B-horizon, and the highest profile masses of clay and Fe_2O_3d. However, the soils have lower profile masses of clay and iron oxides than fans much younger in age. This suggests the upper part of the soil on fan 5 has been stripped or eroded since deposition from post depositional drainages. The morphology of the B-horizon on fan 5 contrasts with younger profiles. For example, soils formed on fans 3 and 4 have developed, thick, fine-grained argillic B-horizon over a coarse-grained C horizon. However, on fan 5 the B-horizon is weakly developed, thin and is composed mainly of coarse grained clasts which continue in similar abundance through the C horizon (Table 2).

The current location of fan 5 and low profile mass values suggest fan 5 could have been modified or originated from Pallett Creek during its offset history along the San Andreas fault (Fig. 2). Fan 5 has been mapped by Barrows et al. (1985) as

boulder gravels belonging to Pallett Creek and not LRC. Currently, fan 5 is displaced ~3 km from the point where it would have blocked the course of Pallett creek onto the floor of the western Mojave Desert, suggesting a source from Pallett Creek. However, Matmon et al. (2005) noted that Pallett Creek exits the mountain front ~3 km south of the San Andreas fault and would deposit coarse sediments south of the San Andreas Fault, whereas LRC exits the mountain front at the fault and deposits coarse sediment north of the fault. Matmon et al. (2005) believed the boulders now exposed on the surface of fan 5 to have originated from LRC and were brought to the surface through continued surficial erosion of overlying soils. Additionally, the age of fan 5 of 413 ka calculated from ^{26}Al and ^{10}Be concentrations in buried sand samples and the distance offset from LRC agrees with other estimated Quaternary slip rates along the Mojave section of the San Andrea fault (Sieh et al., 1984; Salyards et al., 1992; Weldon et al., 1993). This indicates that Matmon et al. (2005) correctly identified fan 5 boulders to originate from LRC and therefore low profile mass values are due to increased erosion and not a Pallett Creek influence or source.

The apparent lack of soil development on fan 5 could also be attributed to the crossing a pedogenic threshold between fans 4 and 5. Pedogenic thresholds have been recognized to explain rapid changes in the rate of development (Muhs, 1984; McFadden and Weldon, 1987; Harrison et al., 1990; Birkeland, 1999). In early stages

of soil development, the coarse soils of fan 5 were well drained. As soil development progressed and more clay was incorporated into the profile through illuviation, weathering, and eolian dust, infiltration rates decreased from reduced porosities and surface runoff increased. Eventually the soil may have crossed a pedogenic threshold where surface erosion was greater than the rate of soil development. The increased runoff due to elevated clay content resulted in accelerated surficial erosion of the thick well developed B-horizon down to the relatively unweathered coarse material below. This would explain thinned B-horizons, coarseness of the profile and lowered profile masses of clay and iron oxides on fan 5. Previous workers have shown the link between increased runoff through the incorporation of fines into a soil profile may result in increased surface erosion (Wells et al., 1987). McFadden (1982) showed that as B-horizon thicknesses decrease due to soil erosion, maximum Fe_2O_3d percent should continue to increase with time as long as hydromorphic conditions do not affect the profile. The slight increase of maximum Fe_2O_3d percent (1.34) of fan 5 compared to fan 4 (1.32) suggests an increase in age even though the profile has been significantly eroded.

Soils and erosion rates

Erosion rates on the LRC fan decrease with increasing age (Matmon et al., in press). This suggests that soils should record changing erosion rates by the presence

of paleosols. Based on the hypothesis of fan development at LRC, young fans with high surface relief should have high erosion rates that would fill in topographic low surfaces (Matmon et al., in press). Soils formed in the topographic low fan surfaces would be eventually buried by the increased sediment flux and would be expressed in the soil profile as a paleosol. However, at LRC topographic low soil profiles lack any paleosols. This suggests that changing erosion rates from the evolution of fan surfaces or large scale climate change does not provide enough sediment to bury surface soils.

Limitations of the chronosequence and estimated age of fan 2

The soil chronofunctions created at LRC should be viewed as semi-quantitative for several reasons. First, the chronofunction curves were created with limited number of data points that have uncertainties associated with fan ages. Only five soil profiles were used to create each curve because fan 2 was not dated and fan 5 has experienced increased erosion from the crossing of a pedogenic threshold. Next, each fan surface might also experience systematic and/or random spatial soil variability (Harrison et al., 1990; Schaetzl et al., 1994). The placement of only one soil profile on each fan surface could mask the overall trend of soil development of each surface if soils vary across a surface. Adding additional soil profiles across each fan surface would help account for soil variability and would build a more robust dataset to create chronofunctions. More soil profiles on fan 5 would also help verify if

the surface has crossed of a pedogenic threshold. Several topographic low soil profiles are not exposed completely to the C horizon (LRC8, LRC10, and LRC12; Table 2) due to limitations of the truck mounted backhoe. This would result in minimum B-horizon thicknesses and lower than actual profile masses of clay and iron oxides, which would influence the resulting soil chronofunctions. Finally, younger fan surfaces have also been disturbed by recreational off-road vehicles and garbage dumping. Although great discretion was used in selecting soil profile sites, off-road vehicles may have disturbed fan surfaces and resulting profile masses and soil chronofunctions of the chronosequence. Despite these uncertainties, clear trends emerge showing the soils at LRC increase in development with increasing age and distance from LRC.

The age of fan 2 was estimated using the solutions of the chronofunctions derived from soil properties on topographic high and low surfaces. Calculated slip rates and offset distances are summarized in Table 3. The slip rates and offset distances constrain the age of fan 2 between 102 – 259 ka. The large age ranges are due to uncertainties in the slip rates and calculated fan ages. Most soil properties yield ages too low for fan 2 when calculating solutions for the soil chronofunctions (Table 3). This could be due to increased soil erosion resulting from drainages developed

after deposition and off-road vehicle activities. Only profile mass of Fe_2O_3d on the topographic low surface produced a reasonable date for fan 2 of 109 ka. However,

Table 3. Summary of fan parameters and estimated ages of fan 2 from solved soil chronofunctions and slip rate data

Source:Matmon et al. (2005); Matmon et al. (in press)	Fan 0	Fan 1	Fan 2	Fan 3	Fan 4	Fan 5
Offset Distance (km)	0.68 ± 0.25	1.75 ± 0.25	5.18 ± 0.55	7.40 ± 0.55	9.60 ± 0.55	16.50 ± 0.55
Erosion Rate (mm/kyr)	17.5 ± 2.2	17.5 ± 2.2	48.4 ± 6.3	41.2 ± 5.4	27.7 ± 3.6	11.3 ± 1.5
Cosmogenic Date (ka)	15.7 ± 5.3	29.5 ± 7.4	no date; > 60	227.4 ± 242	281.4 ± 181	412.8 ± 185
Slip Rate (cm/yr)	4.36 ± 2.17	5.94 ± 1.70	no rate	3.26 ± 3.50	3.41 ± 2.23	4.00 ± 1.81

Source:Matmon et al. (2005)	Slip rate (cm/yr)	Age Range (ka)
Average LRC Slip Rate	4.2 ± 0.9	101.6 - 123.3 - 157.0
Linear Regression Slip Rate	3.7 ± 1.0	110.2 - 140.0 - 191.9
Most Probable Slip Rate	3.0 ± 1.0	129.5 - 172.7 - 259.0

Source: this study		
Topographic highs	Age (ka)	Comments
∑Clay	76.9	age too low for slip rate constraints
$\sum Fe_2O_3d$	41.6	age too low for slip rate constraints
$\sum Fe_2O_3o$	35.0	age too low for slip rate constraints
Topographic lows		
∑Clay	26.9	age too low for slip rate constraints
$\sum Fe_2O_3d$	109.0	within slip rate constraints
$\sum Fe_2O_3o$	55.0	age too low for slip rate constraints

since most soil properties yield ages much too young for fan 2, it can be assumed that the fan's surface has been significantly disturbed. The fan also contains elevated amounts of coarse material, which suggests the profile has been eroded. Matmon et al. (2005) excluded fan 2 from cosmogenic dating because it was believed drainages had modified the surface. The low ages of fan 2 may also reflect the limitation of creating

chronofunctions with limited data points or solving for an unknown independent variable (time) using known dependent variables (soil properties). Williams (1983) stressed this application of a regression equation as a common type of misuse in the geosciences since there isn't perfect correlation between variables. Birkeland (1999) also argued the current understanding of soil chronosequences is not that precise. The lack of reasonable ages for fan 2 also shows the need to carefully evaluate potential sites used in soil chronosequence studies. Even though the chronofunctions underestimate the age of fan 2, they still produce an age greater than that of fan 1. The less than expected ages for fan 2 may also show the value in using chronosequence studies to evaluate whether a surface has experienced significant regressive pedogenesis.

Wider significance

As Johnson et al. (1990) described in the dynamic-rate model of pedogenesis, soils are a product of ongoing pedogenic processes and regressive forces (e.g., erosion), which decrease soil development. In this study there are data on both these processes. The ongoing weathering of soils as seen in the development and thickening of B-horizons, clay and iron oxide accumulations represent progressive soil development. Erosion rates calculated from cosmogenic studies (Matmon et al., 2005;

Matmon et al., in press) represent regressive soil development. Thus, the amount of surface lowering can be calculated over the duration of the chronosequence. The calculated erosion rates decrease from 48.4 ± 6.3 mm/kyr at fan 2 to 11.3 ± 1.5 mm/kyr at fan 5. However, soil data trends to contradict this with erosion rates greater than the rate of soil development on the oldest alluvial fan surface. Also, the rate of soil development changes during the chronosequence with time, as seen in chronofunctions (e.g., clay and iron oxide accumulation). This could also lead to changing erosion rates. Soils on young surfaces should have high infiltration rates which reduce surface runoff and erosion. As soils develop and accumulate clay, infiltration rates should decrease, thus increasing surface runoff and erosion rates. Based on soil data, the highest erosion rates should occur between fans 4 and 5 where the accumulation of clay is the greatest and which is reflected in the significant erosion of soils on fan 5.

The results of this study also provide additional data on the southern California pedogenic gradients and limitations of soil chronosequences. Cajon Pass is the most well-dated and most frequently referenced soil chronosequence in southern California. This study, only 45 km away from Cajon Pass, shows there are significant differences in pedogenic processes between the two areas (e.g., weathering rates, iron oxide accumulation, eolian flux). Other regional studies also show differences in

pedogenic processes between the areas. Cajon Pass would appear to represent a unique soil environment in that it has significant eolian influx.

CONCLUSIONS

Soils in this study increase in development with increasing age and distance from LRC. Soil morphologies change with age by the development and thickening of argillic B-horizons and the accumulation of clay and iron oxides. Additionally, topographic low soils vary more in their clay and iron oxide contents due to inheritance of eroded materials upslope. Clay and iron oxides accumulate similarly to other southern California soil studies along the pedogenic gradient of southern California. However, LRC soils amass less iron oxides than the Cajon Pass chronosequence due to differences in soil forming factors between the areas. This may be attributed to decreased weathering rates from lower temperature, and lower precipitation that would result in lower leaching rates. Additionally, the lack of an eolian influence at LRC would also affect weathering rates. Cajon Pass soils have a large eolian component that increases the water holding capacity of soils, resulting in higher weathering rates. The soils at LRC have less of an eolian input which results in a lower water holding capacity and lower weathering rates.

The soils at LRC also show the importance and limitations of creating a soil chronosequence from a limited number of dated surfaces. Soil chronofunctions created from profile mass of clay and iron oxides of dated fan surfaces, along with

field descriptions, suggests fan 5 has experienced increased erosion due to the crossing of a pedogenic threshold or erosion from the formation of post depositional drainages.

The age of fan 2 cannot be confidently estimated due to erosion from post-depositional drainages and human activities. Lower than expected profile masses of clay and iron oxides show the surface has been eroded. However, the chronosequence may be improved by increasing the number of soil profiles to account for soil variability across surfaces. Additionally, the chronosequence may be used in the future to estimate ages of numerous terrace deposits cut into fan surfaces along the San Andreas fault and strath terraces within the LRC watershed.

REFERENCES

Bailey, R. G., Avers, P. E., King, T., and McNab, W. H., 1994, Ecoregions and Subregions of the United States: U.S. Geological Survey, scale 1:750,000.

Barrows, A. G., Kahle, J. E., and Beeby, D. J., 1985, Earthquake hazards and tectonic history of the San Andreas fault zone, Los Angeles County, California, California Department of Conservation, Division of Mines and Geology, 236 p.

Birkeland, P. W., 1985, Quaternary Soils of the Western United States, *in* Boardman, J., ed., Soils and Quaternary Landscape Evolution: New York, John Wiley & Sons Ltd., p. 303-323.

-, 1999, Soils and Geomorphology: New York, Oxford University Press, 430 p.

Birkeland, P. W., Burke, R. M., and Benedict, J. B., 1989, Pedogenic Gradients for Iron and Aluminum Accumulation and Phosphorus Depletion in Arctic and Alpine Soils as a function of Time and Climate: Quaternary Research, v. 32, p. 193-204.

Bockheim, J. G., 1980, Solution and use of chronofunctions in studying soil development: Geoderma, v. 24, p. 71-85.

Chao, T. T., and Zhou, L., 1983, Extraction techniques for selective dissolution of amorphous iron oxides from soils and sediments: Soil Science Society of America Journal, v. 47, p. 225-232.

Eppes, M. C., 1996, A spatial variability and chronosequence study of soils developing on basalt flows in the Potrillo Volcanic Field, southern New Mexico [M.S. thesis]: New Mexico Institute of Mining and Technology, 110 p.

Eppes, M. C., and Harrison, J. B. J., 1999, Spatial variability of soils developed on basalt flows in the Potrillo Volcanic Field southern New Mexico: prelude to a chronosequence study Earth Surface Processes and Landforms v. 24, p. 1009-1024.

Harden, J. W., 1982, A quantitative index of soil development from field descriptions: examples from a chronosequence in central California: Geoderma, v. 28, p. 1-28.

-, 1987, Soils developed in granitic alluvium near Merced, California: U.S. Geological Survey Bulletin, v. 1590-A, p. 65 p.

Harden, J. W., and Matti, J. C., 1989, Holocene and late Pleistocene slip rates on the San Andreas fault in Yucaipa, California, using displaced alluvial-fan depositys and soil chronology: Geological Society of America Bulletin, v. 101, p. 1107-1117.

Harden, J. W., and Taylor, E. M., 1983, A quantitative comparison of soil development in four climatic regimes: Quaternary Research, v. 20, p. 342-359.

Harrison, J. B. J., McFadden, L. D., and Weldon, R. J., 1990, Spatial soil variability in the Cajon Pass chronosequence: implications for the use of soils as a geochronological tool: Geomorphology, v. 3, p. 399-416.

Holmgren, G. S. S., 1967, A Rapid Citrate-Dithionite Extractable Iron Procedure: Soil Science Society of America Proceedings, v. 31, p. 210-211.

Jenny, H., 1941, Factors of Soil Formation: New York, McGraw-Hill.

-, 1961, Derivation of state factor equations of soils and ecosystems: Soil Science Society of America Proceedings, v. 25, p. 385-388.

Johnson, D. L., Keller, E. A., and Rockwell, T. K., 1990, Dynamic Pedogenesis: New Views on Some Key Soil Concepts, and a Model for Interpreting Quaternary Soils: Quaternary Research, v. 33, p. 1-14.

Kendrick, K. J., and McFadden, L. D., 1996, Comparison and contrast of processes of soil formation in the San Timoteo Badlands with chronosequences in California: Quaternary Research, v. 46, p. 149-160.

Lee, R., Taylor, M. D., and Daly, B. K., 1989, The extraction of Al, Fe and Si from a range of New Zealand soils by hydroxylamine and ammonium oxalate solutions: Australian Journal of Soil Research, v. 27, p. 377-388.

Matmon, A., Nichols, K., and Finkel, B., in press, Evolution of bar and channel topography to smooth surface topography of abandoned fan surfaces, southern California: Quaternary Research.

Matmon, A., Schwartz, D., Finkel, B., Clemmens, S., and Hanks, T., 2005, Dating offset fans along the Mojave section of the San Andreas fault using cosmogenic ^{26}Al and ^{10}Be: Geological Society of America Bulletin, v. 117, p. 795-807.

McFadden, L. D., 1982, The Impact of Temporal and Spatial Climatic Change on Alluvial Soils Genesis in Southern California [PhD dissertation thesis]: University of Arizona, 430 p.

McFadden, L. D., and Hendricks, D. M., 1985, Changes in the Content and Composition of Pedogenic Iron Oxyhydroxides in a Chronosequence of Soils in Southern California: Quaternary Research, v. 23, p. 189-204.

McFadden, L. D., and Weldon, R. J., 1987, Rates and processes of soil development of Quaternary terraces in Cajon Pass, California: Geological Society of America Bulletin, v. 98, p. 280-293.

Muhs, D. R., 1982, A soil chronosequence on Quaternary marine terraces, San Clemente Island, California: Geoderma, v. 28, p. 257-283.

-, 1984, Intrinsic thresholds in soil systems: Physical Geography, v. 5, no. 2, p. 99-110.

Reheis, M., Goodmacher, J. C., Harden, J. W., McFadden, L. D., Shroba, R. R., Sowers, J. M., and Taylor, E. M., 1995, Quaternary soils and dust deposition in southern Nevada and California: Geological Society of America Bulletin, v. 107, p. 1003-1022.

Ross, G. J., Wang, C., and Schuppli, P. A., 1985, Hydroxylamine and ammonium oxalate solutions as extractants for iron and aluminum from soils: Soil Science Society of America Journal, v. 49, p. 783-785.

Salyards, S. L., Sieh, K. E., and Kirschvink, J. L., 1992, Paleomagnetic measurement of nonbrittle coseismic deformation across the San Andreas Fault at Pallett Creek: Journal of Geophysical Research, B, Solid Earth and Planets, v. 97, p. 12457-12470.

Schaetzl, R. J., Barrett, L. R., and Winkler, J. A., 1994, Choosing models for soil chronofunctions and fitting them to data: European Journal of Soil Science, v. 45, p. 219-232.

Schwertmann, U., 1993, Relations between iron oxides, soil color and soil formation: Soil Science Society of America Special Publication no. 31, p. 51-69.

Sieh, K. E., and Jahns, R. H., 1984, Holocene activity of the San Andreas Fault at Wallace Creek: Geological Society of America Bulletin, v. 95, p. 883-896.

Singer, M. J., 1986, Bulk density-paraffin clod method, *in* Singer, M. J., and Janitsky, P., eds., Field and Laboratory Procedures used in a Soil Chronosequence Study, U.S. Geological Survey Bulletin, p. 18-19.

Tedrow, J. C. F., 1977, Soils of the Polar Landscapes: New Brunswick, NJ, Rutgers University Press.

Weldon, R. J., Meisling, K. E., and Alexander, J., 1993, A speculative history of the San Andreas Fault in the central Transverse Ranges, California, *in* Powell, R. E., Weldon, R. J., and Matti, J. C., eds., The San Andreas Fault System: Displacement, Palinspastic Reconstruction and Geologic Evolution: Boulder Colorado, Geological Society of America Memoir 178, p. 161-198.

Weldon, R. J., and Sieh, K. E., 1985, Holocene rate of slip and tentative recurrence interval for large earthquakes on the San Andreas fault, Cajon Pass, southern California: Geological Society of America Bulletin, v. 96, p. 793-812.

Wells, S. G., McFadden, L. D., and Dohrenwend, J. C., 1987, Influence of Late Quaternary Climatic Changes on Geomorphic and Pedogenic Processes on a Desert Piedmont, Eastern Mojave Desert, California: Quaternary Research, v. 27, p. 130-146.

Williams, G. P., 1983, Improper use of regression equations in earth sciences: Geology, v. 11, p. 195-197.

Yaalon, D. H., 1971, Soil-forming processes in space and time, *in* Yaalon, D. H., ed., Paleopedology - Origin, Nature, and Dating of Paleosols: Jerusalem, Israel Universities Press, p. 29-39.

APPENDICES

APPENDIX A - Iron Oxide Extraction Methods and Laboratory Data

Two iron oxide extraction methods were used in this study. First, total secondary iron oxides (Fe_2O_3d) were extracted using the concentrated citrate-dithionite method of Holmgren (1967). The iron oxides extracted from the concentrated citrate-dithionite method are formed from the oxidation of ferric Fe^{2+} to ferrous Fe^{3+} and include: hematite, goethite, ferrihydrite, and some lepidocrocite (McFadden, 1982). The second method extracted poorly crystalline and amorphous secondary iron oxides (Fe_2O_3o) were extracted using the hydroxylamine extractable iron procedure Chao and Zhou (1983). The secondary iron oxide primarily dissolved from this method is ferrihydrite, which is a precursor of hematite. Other iron oxides, such as hematite are not dissolved by this method. Laboratory data are shown in Table 4.

Concentrated citrate-dithionite method:

First, soil samples were crushed and passed through a 100-mesh sieve. Samples were then oven dried overnight to remove water weight. Approximately 0.500 ± 0.100g of each dried and sieved sample was placed into a labeled centrifuge tube. Then, 0.4g of Sodium Dithionite ($Na_2S_3O_4$) was added to each tube. Next, the extraction solution was produced in a 1 liter flask using 200 g of Sodium Citrate ($Na_3C_6H_5O_7 \times 2H_2O$) diluted to 1 liter with ultra-pure water. 25 ml of the sodium

citrate extractant solution was pipetted into each centrifuge tube and then sealed. Each tube was placed on a shaking table for 16 hours. The sample tubes were then centrifuged for 20 minutes at 4000 RPM. Centrifuged samples were then analyzed using an Instrumentation Laboratory Video 12 Flame Atomic Absorption Flame Spectrometer at the New Mexico Bureau of Geology and Mineral Resources. The atomic absorption flame spectrometer was calibrated using 6 standards created from 1000 ppm iron oxide standard and the remaining sodium citrate standard. Concentrations (in parts per million) were recorded (from 5 readings) and then converted to weight percents using a computer spreadsheet program. An example calculation is shown below.

Example Calculation:

Dried sample weighed **513.6mg**

atomic absorption flame spectrometer concentration of **133.7 μg/ml (ppm)**

Iron weight percent Fe_d:

Fe_d % = [concentration (ppm) × extractant solution amount (25 ml) × dilution factor (1) × 100] ÷ [sample weight (mg) × 1000]

[133.7 × 25 × 1 × 100] ÷ [513.6 × 1000] = **0.65 % Fed**

Total secondary iron weight percent Fe_2O_3d:

Fe_2O_3d % = Fe_d % × 1.4297

$Fe_2O_3d\ \% = 0.65 \times 1.4297 =$ **0.929 %**

Hydroxylamine method:

First, soil samples were crushed and passed through a 100-mesh sieve. Samples were then oven dried overnight to remove water weight. Approximately 0.100 ± 0.02g of each dried and sieved sample was placed into a labeled centrifuge tube. Next, the extraction solution was produced in a 2 liter flask by combining 34.74g of hydroxylamine hydrochloride ($NH_2OH \times HCl$) with 41.3ml of 12.1M HCl diluted to the 2 liter mark with ultra-pure water. 25 ml of the hydroxylamine hydrochloride-HCl extractant solution was pipetted into each centrifuge tube and then sealed. Each tube was placed on a shaking table for 16 hours. The sample tubes were then centrifuged for 10 minutes at 2000 RPM. Centrifuged samples were then analyzed using an Instrumentation Laboratory Video 12 Flame Atomic Absorption Flame Spectrometer at the New Mexico Bureau of Geology and Mineral Resources. The atomic absorption flame spectrometer was calibrated using 6 standards created from 1000 ppm iron oxide standard and the remaining hydroxylamine hydrochloride-HCl. Concentrations (in parts per million) were recorded (from 5 readings) and then converted to weight percents using a computer spreadsheet program. An example calculation is shown below.

Example Calculation:

Dried sample weighed **125mg**

Atomic absorption flame spectrometer concentration of **9.3 μg/ml (ppm)**

To get poorly crystalline / amorphous secondary iron weight percent

(Fe_2O_3o):

Fe_o % = [concentration (ppm) × extractant solution amount (25 ml) × dilution factor (1) × 100] ÷ [sample weight (mg) × 1000]

[9.3 × 25 × 1 × 100] ÷ [125 × 1000] = **0.186 % Fe_2O_3o**

Table 4. Fe_2O_3d and Fe_2O_3o Laboratory Data

Sample	Fe_2O_3d Extraction				Duplicate Fe_2O_3o	Fe_2O_3o Extraction		
	Weight (mg)	Fe µg/ml (ppm)	Fe_d %	Fe_2O_3d %		Weight (mg)	Fe µg/ml (ppm)	Fe_2O_3o %
LRC1	513.6	133.7	0.65	0.93		125.0	9.3	0.186
LRC2	509.0	110.2	0.54	0.77		115.6	8.5	0.184
LRC3	529.2	100.3	0.47	0.68		116.1	8.8	0.189
LRC4	554.7	88.1	0.40	0.57		109.4	8.9	0.203
LRC5	518.1	82.5	0.40	0.57		117.2	7.6	0.162
LRC6	555.7	104.9	0.47	0.67		118.7	8.3	0.175
LRC7	525.0	112.9	0.54	0.77		109.1	15.3	0.351
LRC8	500.5	95.3	0.48	0.68		124.5	12.7	0.255
LRC9	485.2	144.5	0.74	1.06		116.8	7.0	0.150
LRC10	527.6	141.7	0.67	0.96		117.6	9.3	0.198
LRC11	565.2	160.1	0.71	1.01		123.0	9.7	0.197
LRC12	500.4	134.6	0.67	0.96		109.4	13.5	0.309
LRC13	537.4	125.4	0.58	0.83		110.6	30.9	0.698
LRC14	543.5	127.2	0.59	0.84		119.7	43.7	0.913
LRC15	545.6	121.5	0.56	0.80		116.1	14.6	0.314
LRC16	522.9	153.1	0.73	1.05		120.8	7.5	0.155
LRC17	512.7	147.3	0.72	1.03		111.1	6.3	0.142
LRC18	506.9	149.5	0.74	1.05		106.7	5.9	0.138
LRC19	495.8	156.6	0.79	1.13		116.5	10.9	0.234
LRC20	515.8	146.5	0.71	1.02		102.8	7.8	0.190
LRC21	489.2	131.3	0.67	0.96		117.2	10.2	0.218
LRC22	489.8	131.5	0.67	0.96		114.1	10.9	0.239
LRC23	515.4	134.9	0.65	0.94		107.8	10.6	0.246
LRC24	528.5	150.8	0.71	1.02		125.4	9.8	0.195
LRC25	507.0	134.3	0.66	0.95		107.1	10.0	0.233
LRC26	507.3	175.3	0.86	1.24		103.3	23.3	0.564
LRC27	526.8	167.7	0.80	1.14		117.1	39.8	0.850
LRC28	532.4	143.4	0.67	0.96		110.5	33.4	0.756
LRC29	508.6	127.2	0.63	0.89		123.8	47.1	0.951
LRC30	505.1	116.9	0.58	0.83		119.3	43.6	0.914
LRC31	526.9	117.6	0.56	0.80		133.0	46.6	0.876
LRC32	537.0	126.2	0.59	0.84		110.5	24.3	0.550

Table 4 Continued. Fe_2O_3d and Fe_2O_3o Laboratory Data

Sample	Fe_2O_3d Extraction				Duplicate	Fe_2O_3o Extraction		
	Weight (mg)	Fe µg/ml (ppm)	Fe_d %	Fe_2O_3d %	Fe_2O_3o	Weight (mg)	Fe µg/ml (ppm)	Fe_2O_3o %
LRC33	500.2	101.3	0.51	0.72		122.3	7.7	0.157
LRC34	493.9	143.7	0.73	1.04		113.7	10.4	0.229
LRC35	497.2	163.2	0.82	1.17		118.8	16.0	0.337
LRC36	532.2	157.3	0.74	1.06		119.8	18.9	0.394
LRC37	522.4	117.5	0.56	0.80		111.3	14.8	0.332
LRC38	506.0	99.1	0.49	0.70		135.0	16.2	0.300
LRC39	541.5	96.8	0.45	0.64		110.6	12.4	0.280
LRC40	501.4	144.1	0.72	1.03		115.5	11.4	0.247
LRC41	494.2	153.0	0.77	1.11		118.1	12.1	0.256
LRC42	494.0	190.2	0.96	1.38		108.9	23.6	0.542
LRC43	474.1	187.7	0.99	1.42		117.9	79.3	1.682
LRC44	509.3	161.0	0.79	1.13		116.2	58.9	1.267
LRC45	492.0	164.0	0.83	1.19		112.4	58.4	1.299
LRC46	507.3	160.7	0.79	1.13		110.8	53.7	1.212
LRC47	508.0	140.6	0.69	0.99		119.8	20.3	0.424
LRC48	532.9	146.5	0.69	0.98		105.1	20.4	0.485
LRC49	607.5	118.9	0.49	0.70		122.5	6.5	0.133
LRC50	493.6	134.3	0.68	0.97		113.1	6.9	0.153
LRC51	505.8	118.7	0.59	0.84		109.0	6.0	0.138
LRC52	525.5	139.9	0.67	0.95		127.5	8.3	0.163
LRC53	570.1	142.7	0.63	0.89		113.1	8.4	0.186
LRC54	502.8	143.9	0.72	1.02		115.7	12.6	0.272
LRC55	497.9	159.1	0.80	1.14		125.3	15.5	0.309
LRC56	486.9	157.5	0.81	1.16		119.0	13.1	0.275
LRC57	486.9	158.2	0.81	1.16		115.7	13.6	0.294
LRC58	502.3	135.6	0.67	0.96		113.9	8.0	0.176
LRC59	473.7	141.3	0.75	1.07		111.4	10.9	0.245
LRC60	505.1	186.7	0.92	1.32		111.1	17.4	0.392
LRC61	499.6	164.8	0.82	1.18		115.4	26.2	0.568
LRC62	499.5	173.9	0.87	1.24		111.6	25.5	0.571
LRC63	513.3	175.2	0.85	1.22		110.9	20.3	0.458
LRC64	516.9	156.9	0.76	1.08		115.3	19.9	0.431
LRC65	495.8	136.5	0.69	0.98		113.4	17.5	0.386

Table 4 Continued. Fe_2O_3d and Fe_2O_3o Laboratory Data

Sample	Fe_2O_3d Extraction				Duplicate Fe_2O_3o	Fe_2O_3o Extraction		
	Weight (mg)	Fe µg/ml (ppm)	Fe_d %	Fe_2O_3d %		Weight (mg)	Fe µg/ml (ppm)	Fe_2O_3o %
LRC66	535.2	118.0	0.55	0.79		116.6	5.6	0.120
LRC67	495.0	134.8	0.68	0.97		131.8	7.7	0.146
LRC68	506.5	163.1	0.81	1.15		125.3	10.7	0.213
LRC69	505.0	159.6	0.79	1.13		111.1	10.7	0.241
LRC70	491.6	146.8	0.75	1.07		113.8	13.0	0.286
LRC71	500.1	149.6	0.75	1.07		116.9	14.1	0.302
LRC72	500.4	141.4	0.71	1.01		121.7	13.9	0.286
LRC73	499.8	152.3	0.76	1.09		127.8	12.3	0.241
LRC74	516.9	151.7	0.73	1.05		130.8	11.9	0.227
LRC75	544.1	165.0	0.76	1.08		104.2	9.9	0.238
LRC76	510.3	165.0	0.81	1.16		114.1	17.1	0.375
LRC77	506.1	171.4	0.85	1.21		117.4	20.3	0.432
LRC78	501.4	187.5	0.93	1.34		105.5	21.7	0.514
LRC79	498.6	176.1	0.88	1.26		127.6	25.9	0.507
LRC80	506.0	158.4	0.78	1.12		116.5	20.1	0.431
LRC81	496.6	142.6	0.72	1.03		118.0	15.6	0.331
LRC82	517.2	123.6	0.60	0.85		124.5	6.7	0.135
LRC83	542.9	158.9	0.73	1.05		101.3	7.7	0.190
LRC84	491.2	146.6	0.75	1.07		116.8	9.0	0.193
LRC85	512.6	156.8	0.76	1.09		112.6	9.3	0.206
LRC86	503.8	145.4	0.72	1.03		113.0	9.5	0.210
LRC87	498.9	152.5	0.76	1.09		112.0	10.6	0.237
LRC88	515.6	158.2	0.77	1.10		101.0	11.3	0.280
LRC89	490.8	164.2	0.84	1.20		122.3	20.0	0.409
LRC90	512.3	169.9	0.83	1.19		116.1	17.0	0.366
LRC91	492.3	182.9	0.93	1.33		109.1	9.2	0.211
LRC92	493.5	192.4	0.97	1.39		104.3	15.2	0.364
LRC93	497.9	196.2	0.99	1.41		119.0	25.1	0.527
LRC94	499.5	193.8	0.97	1.39		112.6	17.4	0.386
LRC95	511.6	152.8	0.75	1.07		109.8	9.6	0.219
LRC96	509.9	172.9	0.85	1.21		126.9	14.0	0.276
LRC97	519.2	88.9	0.43	0.61		109.2	7.1	0.163
LRC98	539.5	102.9	0.48	0.68		125.2	8.8	0.176
LRC99	539.9	90.5	0.42	0.60		143.0	10.3	0.180
LRC100	537.0	115.8	0.54	0.77		138.0	10.4	0.188
LRC101	516.8	84.3	0.41	0.58		127.9	10.5	0.205
LRC102	571.5	84.6	0.37	0.53		153.6	11.4	0.186
LRC103	501.7	99.3	0.49	0.71		121.7	13.5	0.277
LRC104	526.9	107.7	0.51	0.73		118.9	14.6	0.307

Table 4 Continued. Fe_2O_3d and Fe_2O_3o Laboratory Data

Sample	Fe_2O_3d Extraction				Duplicate	Fe_2O_{3o} Extraction		
	Weight (mg)	Fe µg/ml (ppm)	Fe_d %	Fe_2O_3d %	Fe_2O_{3o}	Weight (mg)	Fe µg/ml (ppm)	Fe_2O_{3o} %
LRC5-2	494.0	73.2	0.37	0.53	LRC23-2	112.3	10.5	0.234
LRC13-2	528.0	120.3	0.57	0.81	LRC23-3	94.0	9.5	0.253
LRC27-2	501.8	142.2	0.71	1.01	LRC82-2	102.0	5.5	0.135
LRC46-2	502.1	167.9	0.84	1.20	LRC57-2	109.8	20.4	0.464
LRC64-2	517.4	159.2	0.77	1.10				
LRC75-2	502.9	155.3	0.77	1.10				
LRC34-2	536.0	159.6	0.74	1.06				
LRC66-2	503.0	113.0	0.56	0.80				
LRC87-2	478.2	141.5	0.74	1.06				

APPENDIX B - Calculation of horizon and profile mass

The total profile mass of clay, Fe_2O_3d, and Fe_2O_3o were calculated similarly to the method used by McFadden and Hendricks (1985). However, C horizon profile mass was not subtracted from profile masses in this study because some profiles did not reach the C horizon. Field and laboratory of Fe_2O_3d data from soil profile LRC 7 (Table 5) are used below as an example of the calculations of horizon and profile masses. Actual calculations were performed using a computer spreadsheet.

Table 5. Selected field and laboratory data used for and example calculation of horizon and profile mass.

Soil Profile	Sample Number	Profile Horizon	Depth (cm)	Gravel %	Stones & Cobbles %	Total Gravels (%)	Fe_2O_3d (%)	Horizon Thickness (cm)	Bulk Density (g/cm^3)	Horizon Mass Fe_2O_3d (g)	Profile Mass Fe_2O_3d (g)
LRC7	LRC40	A	0-8	15	11	26	1.03	8	1.20	0.07	1.67
	LRC41	AB	8-14	20	11	31	1.11	6	1.51	0.07	
	LRC42	Bt1(1)	14-35	30	16	46	1.38	21	1.81	0.28	
	LRC43	Bt1(2)	35-50	30	16	46	1.42	15	1.81	0.21	
	LRC44	Bt2(1)	50-70	35	11	46	1.13	20	1.67	0.20	
	LRC45	Bt2(2)	70-95	35	11	46	1.19	25	1.74	0.28	
	LRC46	2BC	95-135	20	17	37	1.13	40	1.95	0.56	
	LRC47	3C	135-153	30	18	48	0.99	18	1.88	0.17	
	LRC48	4C	153-180	70	18	88	0.98	27	1.92	0.06	

Horizon mass (g) = [horizon bulk density (g/cm^3)] × [weight % of soil property] × [1 – % total gravels] × [horizon thickness (cm)]

Profile mass (g) = $\sum$ (all horizon above the C horizon)

Example of horizon mass using sample LRC40:

Horizon mass (g) = [1.20 (g/cm^3)] × [0.0103] × [1 – .26] × [8 (cm)]
= 0.07

Example of profile mass using soil profile LRC7:

Profile mass (g) = 0.07 + 0.07 + 0.28 + 0.21 + 0.20 + 0.28 + 0.56
= 1.67

Table 6 below shows the numbers used in the calculations of horizon and profile mass of sand, silt, clay, Fe_2O_3d, and Fe_2O_3o. Resulting profile masses were used to create figures discussed in the text. Profile masses for the trench site at fan 5 (LRC 91-96) were not calculated because of limited profile data.

Table 6. Expanded table of calculations for horizon and profile mass of sand, silt, clay, Fe_2O_3d, and Fe_2O_3o.

	Total	Particle size, <2 mm					Horizon	Bulk	Horizon Mass (g)					Total Profile Mass (g)				
Sample Number	Gravels (%)	Sand (%)	Silt (%)	Clay (%)	Fe_2O_3d (%)	Fe_2O_3o (%)	Thickness (cm)	Density (g/cm^3)	Sand	Silt	Clay	Fe_2O_3d	Fe_2O_3o	Sand	Silt	Clay	Fe_2O_3d	Fe_2O_3o
LRC97	27	93.96	5.51	0.53	0.61	0.16	5	1.43	4.90	0.29	0.03	0.03	0.01	4.90	0.29	0.03	0.03	0.01
LRC98	15	97.24	1.76	1.00	0.68	0.18	5	1.46	6.03	0.11	0.06	0.04	0.01					
LRC99	15	97.12	2.59	0.29	0.60	0.18	5	1.54	6.36	0.17	0.02	0.04	0.01					
LRC100	15	97.09	2.41	0.50	0.77	0.19	5	1.40	5.78	0.14	0.03	0.05	0.01					
LRC101	30	96.88	2.38	0.74	0.58	0.21	5	1.37	4.65	0.11	0.04	0.03	0.01					
LRC102	56	96.21	2.67	1.12	0.53	0.19	5	1.37	2.90	0.08	0.03	0.02	0.01					
LRC103	53	91.80	6.90	1.31	0.71	0.28	5	1.26	2.72	0.20	0.04	0.02	0.01					
LRC104	28	86.32	9.27	4.41	0.73	0.31	5	1.11	3.45	0.37	0.18	0.03	0.01					
LRC1	15	73.94	21.95	4.10	0.93	0.19	12	1.57	11.80	3.50	0.65	0.15	0.03	49.63	10.13	2.56	0.47	0.12
LRC2	60	76.38	18.24	5.38	0.77	0.18	18	1.57	8.61	2.06	0.61	0.09	0.02					
LRC3	33	83.28	13.03	3.69	0.68	0.19	34	1.54	29.22	4.57	1.29	0.24	0.07					
LRC4	51	90.17	8.15	1.68	0.57	0.20	16	1.54	10.89	0.98	0.20	0.07	0.02					
LRC5	51	90.76	5.18	4.07	0.57	0.16	20	1.52	13.52	0.77	0.61	0.08	0.02					
LRC6	15	75.52	16.85	7.63	0.67	0.17	7	1.50	6.74	1.50	0.68	0.06	0.02	21.31	4.64	1.97	0.21	0.08
LRC7	10	76.74	16.50	6.77	0.77	0.35	13	1.62	14.57	3.13	1.28	0.15	0.07					
LRC8	5	76.91	15.38	7.71	0.68	0.26	20	1.79	26.23	5.25	2.63	0.23	0.09					
LRC9	3	93.22	4.82	1.96	1.06	0.15	5	1.79	8.09	0.42	0.17	0.09	0.01					
LRC10	22	74.21	20.33	5.46	0.96	0.20	5	1.42	4.10	1.12	0.30	0.05	0.01	99.23	24.84	7.53	1.19	0.65
LRC11	12	75.43	17.94	6.63	1.01	0.20	18	1.66	19.83	4.72	1.74	0.27	0.05					
LRC12	25	74.33	18.72	6.95	0.96	0.31	27	1.61	24.16	6.08	2.26	0.31	0.10					
LRC13	25	78.82	15.87	5.31	0.83	0.70	15	1.45	12.86	2.59	0.87	0.14	0.11					
LRC14	5	76.62	19.15	4.22	0.84	0.91	23	1.59	26.62	6.65	1.47	0.29	0.32					
LRC15	5	71.82	22.65	5.53	0.80	0.31	10	1.71	11.67	3.68	0.90	0.13	0.05					
LRC16	5	80.62	16.64	2.74	1.05	0.16	20	1.83	28.03	5.79	0.95	0.36	0.05					
LRC17	3	66.02	24.41	9.57	1.03	0.14	10	1.70	10.90	4.03	1.58	0.17	0.02	82.73	23.48	13.68	1.27	0.21
LRC18	2	76.09	16.09	7.82	1.05	0.14	25	1.51	28.23	5.97	2.90	0.39	0.05					
LRC19	2	64.83	21.62	13.54	1.13	0.23	20	1.49	18.90	6.30	3.95	0.33	0.07					
LRC20	2	66.52	19.33	14.14	1.02	0.19	25	1.52	24.70	7.18	5.25	0.38	0.07					
LRC21	0	60.87	36.01	3.12	0.96	0.22	20	1.61	19.65	11.63	1.01	0.31	0.07					
LRC22	0	60.83	31.58	7.59	0.96	0.24	30	1.74	31.79	16.50	3.97	0.50	0.12					
LRC23	0	63.26	21.66	15.08	0.94	0.25	30	1.68	31.87	10.91	7.60	0.47	0.12					
LRC24	0	67.76	21.31	10.92	1.02	0.20	40	1.75	47.34	14.89	7.63	0.71	0.14					
LRC25	38	77.12	17.85	5.03	0.95	0.23	12	1.44	8.26	1.91	0.54	0.10	0.03	88.00	14.46	10.40	1.16	0.82
LRC26	28	71.85	14.74	13.41	1.24	0.56	25	1.69	21.86	4.48	4.08	0.38	0.17					
LRC27	25	76.94	12.78	10.28	1.14	0.85	13	1.69	12.64	2.10	1.69	0.19	0.14					
LRC28	25	82.85	8.93	8.22	0.96	0.76	15	1.75	16.26	1.75	1.61	0.19	0.15					
LRC29	40	80.61	11.49	7.89	0.89	0.95	15	1.67	12.12	1.73	1.19	0.13	0.14					
LRC30	40	81.71	12.02	6.25	0.83	0.91	20	1.72	16.86	2.48	1.29	0.17	0.19					
LRC31	75	87.96	8.88	3.15	0.80	0.88	45	1.72	17.02	1.72	0.61	0.15	0.17					
LRC32	55	92.13	4.95	2.91	0.84	0.55	15	1.72	10.70	0.57	0.34	0.10	0.06					
LRC33	15	81.80	14.08	4.11	0.72	0.16	15	1.42	14.86	2.56	0.75	0.13	0.03	128.24	37.60	9.06	1.69	0.56
LRC34	10	74.45	23.48	2.07	1.04	0.23	15	1.60	16.04	5.06	0.45	0.22	0.05					
LRC35	20	70.43	22.44	7.13	1.17	0.34	20	2.08	23.44	7.47	2.37	0.39	0.11					
LRC36	20	73.13	21.04	5.83	1.06	0.39	30	2.01	35.26	10.15	2.81	0.51	0.19					
LRC37	25	71.97	23.04	4.99	0.80	0.33	35	2.05	38.63	12.37	2.68	0.43	0.18					
LRC38	25	69.37	26.71	3.92	0.70	0.30	25	2.05	26.66	10.27		0.27	0.12					
LRC39	15	69.44	26.21	4.35	0.64	0.28	30	2.05	36.30	13.70		0.33	0.15					

Table 6 Continued. Expanded table for calculations of horizon and profile mass of sand, silt, clay, Fe_2O_3d, and Fe_2O_3o.

	Total	Particle size, <2 mm					Horizon	Bulk	Horizon Mass (g)					Total Profile Mass (g)				
Sample Number	Gravels (%)	Sand (%)	Silt (%)	Clay (%)	Fe_2O_3d (%)	Fe_2O_3o (%)	Thickness (cm)	Density (g/cm^3)	Sand	Silt	Clay	Fe_2O_3d	Fe_2O_3o	Sand	Silt	Clay	Fe_2O_3d	Fe_2O_3o
LRC40	26	74.81	17.20	7.98	1.03	0.25	8	1.20	5.31	1.22	0.57	0.07	0.02	101.92	22.76	14.50	1.67	1.52
LRC41	31	71.15	19.80	9.00	1.11	0.26	6	1.51	4.45	1.24	0.56	0.07	0.02					
LRC42	46	63.98	17.50	18.50	1.38	0.54	21	1.81	13.13	3.59	3.80	0.28	0.11					
LRC43	46	61.71	20.74	17.53	1.42	1.68	15	1.81	9.05	3.04	2.57	0.21	0.25					
LRC44	46	68.22	19.85	11.91	1.13	1.27	20	1.67	12.30	3.58	2.15	0.20	0.23					
LRC45	46	77.04	15.49	7.46	1.19	1.30	25	1.74	18.10	3.64	1.75	0.28	0.31					
LRC46	37	80.53	13.13	6.32	1.13	1.21	40	1.95	39.57	6.45	3.11	0.56	0.60					
LRC47	48	87.95	8.37	3.67	0.99	0.42	18	1.88	15.48	1.47	0.65	0.17	0.07					
LRC48	88	84.16	11.92	3.91	0.98	0.49	27	1.92	5.24	0.74	0.24	0.06	0.03					
LRC49	10	60.78	33.63	5.59	0.70	0.13	5	1.34	3.67	2.03	0.34	0.04	0.01	145.05	67.05	25.61	2.42	0.55
LRC50	10	60.57	32.96	6.47	0.97	0.15	9	1.33	6.52	3.55	0.70	0.10	0.02					
LRC51	15	60.76	31.97	7.27	0.84	0.14	16	1.48	12.25	6.45	1.47	0.17	0.03					
LRC52	15	61.28	29.78	8.95	0.95	0.16	30	1.50	23.48	11.41	3.43	0.36	0.06					
LRC53	15	56.19	29.74	14.06	0.89	0.19	30	1.45	20.75	10.98	5.19	0.33	0.07					
LRC54	15	59.28	30.61	10.11	1.02	0.27	20	1.51	15.25	7.87	2.60	0.26	0.07					
LRC55	10	62.98	25.53	11.49	1.14	0.31	30	1.59	27.11	10.99	4.94	0.49	0.13					
LRC56	32	62.11	25.24	12.65	1.16	0.28	30	1.60	20.23	8.22	4.12	0.38	0.09					
LRC57	49	65.35	22.97	11.68	1.16	0.29	30	1.58	15.79	5.55	2.82	0.28	0.07					
LRC58	0	70.68	26.22	3.09	0.96	0.18	10	1.72	12.16	4.51	0.53	0.17	0.03	135.01	37.86	39.16	2.53	0.94
LRC59	7	70.00	22.12	7.87	1.07	0.24	12	1.57	12.26	3.88	1.38	0.19	0.04					
LRC60	10	58.11	18.30	23.57	1.32	0.39	28	1.74	25.48	8.02	10.33	0.58	0.17					
LRC61	10	64.15	15.16	20.69	1.18	0.57	22	1.96	24.90	5.88	8.03	0.46	0.22					
LRC62	35	62.19	14.43	23.37	1.24	0.57	28	2.00	22.64	5.25	8.51	0.45	0.21					
LRC63	41	64.08	15.78	20.13	1.22	0.46	35	1.99	26.33	6.48	8.27	0.50	0.19					
LRC64	68	65.04	22.18	12.18	1.08	0.43	30	1.80	11.24	3.83	2.10	0.19	0.07					
LRC65		77.47	15.37	7.16	0.98	0.39	35	1.80	48.81	9.68	4.51	0.62	0.24					
LRC66	10	83.20	12.93	3.87	0.79	0.12	9	1.52	10.27	1.60	0.48	0.10	0.01	216.44	55.38	24.08	3.18	0.72
LRC67	5	80.10	14.37	5.52	0.97	0.15	8	1.68	10.24	1.84	0.71	0.12	0.02					
LRC68	8	69.94	19.59	10.47	1.15	0.21	33	1.55	32.86	9.20	4.92	0.54	0.10					
LRC69	8	71.96	21.47	6.57	1.13	0.24	35	1.63	37.66	11.24	3.44	0.59	0.13					
LRC70	10	72.59	19.79	7.63	1.07	0.29	15	1.63	16.02	4.37	1.68	0.24	0.06					
LRC71	10	72.59	20.99	6.42	1.07	0.30	14	1.62	14.84	4.29	1.31	0.22	0.06					
LRC72	12	74.25	17.62	8.13	1.01	0.29	31	1.69	34.32	8.14	3.76	0.47	0.13					
LRC73	15	72.81	17.78	9.41	1.09	0.24	55	1.77	60.24	14.71	7.79	0.90	0.20					
LRC74	26	62.37	33.70	3.92	1.05	0.23	12	1.53	8.47	4.58	0.53	0.14	0.03	49.12	16.63	7.79	0.87	0.30
LRC75	87	71.68	21.39	6.93	1.08	0.24	13	1.57	1.90	0.57	0.18	0.03	0.01					
LRC76	82	66.32	21.73	11.94	1.16	0.37	14	1.80	3.01	0.99	0.54	0.05	0.02					
LRC77	52	66.88	21.16	11.95	1.21	0.43	29	1.63	15.17	4.80	2.71	0.27	0.10					
LRC78	62	63.57	21.22	15.19	1.34	0.51	17	1.73	7.10	2.37	1.70	0.15	0.06					
LRC79	62	71.00	17.41	11.60	1.26	0.51	17	1.62	7.43	1.82	1.21	0.13	0.05					
LRC80	77	71.33	17.85	10.80	1.12	0.43	21	1.75	6.03	1.51	0.91	0.09	0.04					
LRC81	77	76.85	7.36	15.79	1.03	0.33	27	1.75	8.35	0.80	1.72	0.11	0.04					
LRC82	12	79.89	17.99	2.12	0.85	0.13	14	1.50	14.76	3.32	0.39	0.16	0.02	219.88	55.27	13.44	3.16	0.78
LRC83	7	77.11	18.45	4.44	1.05	0.19	16	1.60	18.34	4.39	1.06	0.25	0.05					
LRC84	7	78.11	17.84	4.04	1.07	0.19	20	1.53	22.19	5.07	1.15	0.30	0.05					
LRC85	7	77.73	21.73	0.54	1.09	0.21	20	1.41	20.35	5.69	0.14	0.29	0.05					
LRC86	7	78.19	20.09	1.73	1.03	0.21	20	1.61	23.47	6.03	0.52	0.31	0.06					
LRC87	7	78.17	15.56	6.27	1.09	0.24	20	1.61	23.35	4.65	1.87	0.33	0.07					
LRC88	7	76.15	17.35	6.50	1.10	0.28	30	1.58	33.58	7.65	2.87	0.48	0.12					
LRC89	5	71.52	19.33	9.15	1.20	0.41	30	1.56	31.88	8.61	4.08	0.53	0.18					
LRC90	5	74.00	22.82	3.18	1.19	0.37	30	1.52	31.96	9.86	1.37	0.51	0.16					
LRC91		70.42	20.84	8.74	1.33	0.21	22	1.64	25.41	7.52		0.48						
LRC92		65.82	21.42	12.76	1.39	0.36	28	1.49	27.38	8.91		0.58						
LRC93		63.20	21.57	15.23	1.41	0.53	30	1.71	32.39	11.05		0.72						
LRC94		71.23	18.05	10.72	1.39	0.39	30											
LRC95		82.10	8.47	9.43	1.07	0.22	60											
LRC96		83.33	4.20	12.47	1.21	0.28	30											

APPENDIX C - Fan Locations

Table 7. Location of soil profiles along offset alluvial fans near Little Rock, CA

Soil Profile	Fan #	Easting[a]	Northing[a]	Topo location
LRC1	0	406759	3819006	High
LRC2	0	406733	3819003	Low
LRC3	1	408766	3818131	High
LRC4	1	408626	3818179	Low
LRC5	2	410002	3817531	High
LRC6	2	409876	3817608	Low
LRC7	3	408013	3818474	High
LRC8	3	407165[b]	3818876[b]	Low
LRC9	4	414250	3815591	High
LRC10	4	414285	3815601	Low
LRC11	5	420462	3812631	High
LRC12	5	420515	3812808	Low
LRC13	5	420409	3812738	High (Trench site)
LRC14	Active Channel	406934	3819170	LRC Wash

[a]Map datum is UTM NAD 27, Zone 11S, CONUS

[b]Approximate profile location